Global Variational Inference Enhanced Robust Domain Adaptation

Lingkun Luo, Shiqiang Hu, Liming Chen, *Senior member, IEEE*

***Abstract*—Deep learning-based domain adaptation (DA) methods have shown strong performance by learning transferable representations. However, their reliance on mini-batch training limits global distribution modeling, leading to unstable alignment and suboptimal generalization. We propose Global Variational Inference Enhanced Domain Adaptation (GVI-DA), a framework that learns continuous, class-conditional global priors via variational inference to enable structure-aware cross-domain alignment. GVI-DA minimizes domain gaps through latent feature reconstruction, and mitigates posterior collapse using global codebook learning with randomized sampling. It further improves robustness by discarding low-confidence pseudo-labels and generating reliable target-domain samples. Extensive experiments on four benchmarks and thirty-eight DA tasks demonstrate consistent state-of-the-art performance. We also derive the model's evidence lower bound (ELBO) and analyze the effects of prior continuity, codebook size, and pseudo-label noise tolerance. In addition, we compare GVI-DA with diffusion-based generative frameworks in terms of optimization principles and efficiency, highlighting both its theoretical soundness and practical advantages.**

***Index Terms*—Domain Adaptation, Global Variational Inference, Global Continuous Distribution.**

I. Introduction

DEEP learning models have achieved remarkable success by leveraging large-scale, well-annotated datasets $(\mathcal{X}_\mathcal{S}, \mathcal{Y}_\mathcal{S})$, typically under the assumption that training (source domain) and testing (target domain) samples are drawn from a same data distribution. Formally, this corresponds to the *i.i.d.* assumption: $p(\mathcal{X}_\mathcal{S}, \mathcal{Y}_\mathcal{S}) = p(\mathcal{X}_\mathcal{T}, \mathcal{Y}_\mathcal{T})$. However, in real-world scenarios, this *i.i.d.* assumption is often violated due to changes in environment, sensor differences, or data acquisition processes, leading to domain shift: $p(\mathcal{X}_\mathcal{S}, \mathcal{Y}_\mathcal{S}) \neq p(\mathcal{X}_\mathcal{T}, \mathcal{Y}_\mathcal{T})$. This distribution mismatch severely hinders the generalization of source-trained models on target domains. Unsupervised Domain Adaptation (UDA) aims to mitigate this challenge by transferring knowledge from labeled source data $\mathcal{D}_\mathcal{S}$ to unlabeled target data $\mathcal{D}_\mathcal{T}$, despite the domain discrepancy.

While current UDA approaches can be broadly categorized into *shallow* and *deep* domain adaptation (DA) methods, deep learning-based DA (DL-DA) has emerged as the dominant paradigm thanks to its powerful representation learning capabilities, especially in large-scale settings. However, DL-DA models typically rely on batch-based sampling to handle large datasets, which inherently limits them to local views of the data distribution. This localized sampling leads to incomplete modeling of cross-domain distributions, impeding the ability of the model to capture global structural alignments between domains [53], and consequently resulting in looser generalization error bounds.

To rigorously assess the limitations arising from the lack of global knowledge, we revisit the theoretical foundations of UDA as established in [2], [34]. Specifically, Eq. (1) presents an error bound for hypothesis h in the target domain, which serves as a theoretical framework for optimizing models under non-*iid* conditions in cross-domain learning.

$$e_\mathcal{T}(h) \leq \underbrace{e_\mathcal{S}(h)}_{\textbf{Term.1}} + \underbrace{d_H(\mathcal{D}_\mathcal{S}, \mathcal{D}_\mathcal{T})}_{\textbf{Term.2}} + \underbrace{\min\left\{E_{\mathcal{D}_\mathcal{S}}\left[|f_\mathcal{S}(\mathbf{x}) - f_\mathcal{T}(\mathbf{x})|\right], E_{\mathcal{D}_\mathcal{T}}\left[|f_\mathcal{S}(\mathbf{x}) - f_\mathcal{T}(\mathbf{x})|\right]\right\}}_{\textbf{Term.3}}, \tag{1}$$

where the performance $e_\mathcal{T}(h)$ of a hypothesis h on $\mathcal{D}_\mathcal{T}$ is bounded by three critical terms on the right-hand side of Eq. (1). Specifically, **Term.1** represents the classification error on $\mathcal{D}_\mathcal{S}$, **Term.2** quantifies the $\mathcal{H}$-divergence [34] between the cross-domain distributions $\mathcal{D}_\mathcal{S}$ and $\mathcal{D}_\mathcal{T}$, and **Term.3** captures the discrepancy between the labeling functions of the two domains. In the context of UDA, optimizing **Term.1** is typically achieved through supervised learning to ensure effective functional regularization. However, the optimization of **Term.2** and **Term.3** is hindered by the absence of global knowledge modeling inherent to batch learning–based training settings.

- **Term.2** denotes the $\mathcal{H}$-divergence between the source and target domain distributions, formally defined as: $d_\mathcal{H}(\mathcal{D}_\mathcal{S}, \mathcal{D}_\mathcal{T}) = \sup_{h\in\mathcal{H}} |\mathbb{P}_{\mathcal{D}_\mathcal{S}}(h) - \mathbb{P}_{\mathcal{D}_\mathcal{T}}(h)|$. However, in batch-learning-based deep domain adaptation (DL-DA), the estimation of cross-domain divergence inherently relies on mini-batch sampling. As a result, in addition to the global distribution shift between $\mathcal{D}_\mathcal{S}$ and $\mathcal{D}_\mathcal{T}$, one must also account for intra-domain distributional variations introduced by batch sampling. Specifically, the statistical incompleteness across batches can lead to distributional inconsistencies within each domain. This additional variability can be quantified as: $\sum_{i,j\in\{1,\ldots,N\}, i\neq j} \left(d_\mathcal{H}(\mathcal{D}_\mathcal{S}^{B_i}, \mathcal{D}_\mathcal{S}^{B_j}) + d_\mathcal{H}(\mathcal{D}_\mathcal{T}^{B_i}, \mathcal{D}_\mathcal{T}^{B_j})\right)$, where N is the number of training batches, and $\mathcal{D}_\mathcal{S}^{B_i}$, $\mathcal{D}_\mathcal{T}^{B_i}$ denote the sampled distributions from the i-th batch in the source and target domains, respectively. These intra-domain divergence terms reflect the limitations of DL-DA in capturing global distributional structures, thereby affecting the overall stability and effectiveness of domain alignment.
- **Term.3** captures the discrepancy between the labeling functions of the cross domains. In the UDA setting, target domain pseudo-labels are inferred by the source-trained classifier, relying on the assumption that Term.2 has already reduced the domain divergence. Consequently, the optimization of Term.3 is inherently dependent on the success of Term.2. If Term.2 is poorly optimized,

K. Luo and S. Qiang are from Shanghai Jiao Tong University, 800 Dongchuan Road, Shanghai, China e-mail: (lolinkun1988, sqhu)@sjtu.edu.cn; L. Chen from LIRIS, CNRS UMR 5205, Ecole Centrale de Lyon, and Institut Universitaire de France (IUF), 36 avenue Guy de Collongue, Ecully, France e-mail: liming.chen@ec-lyon.fr.

the pseudo-labels in the target domain will be unreliable, thereby limiting the effectiveness of Term.3.

A few methods have been proposed to mitigate the local inconsistency of batch-wise sampling and the lack of global knowledge in domain adaptation. Early approaches such as **DSAN** [92] introduced class-wise sampling to alleviate category-missing bias, while subsequent works like **CAG-UDA** [87], **MiRe** [6], **DRDA** [28], **TransVQA** [65], and **CMA** [73] proposed global anchors or memory mechanisms to unify feature distributions across batches. Among them, **GAN-DA** [53] offers a more unified formulation by aligning source and target feature distributions via projection onto discrete *Predefined Feature Representations* (PFRs), used as global class-wise anchors. However, *rigidly forcing* continuous feature distributions to be projected onto discrete anchors inevitably disregards the intrinsic mismatch between continuous manifolds and discrete fixed prior representations (subsequently denoted as projection gap), thereby failing to model the class-conditional distributions $\phi(x_{\mathcal{S}}, c) \sim \mathcal{P}_{\mathcal{S}}$ and $\phi(x_{\mathcal{T}}, c) \sim \mathcal{P}_{\mathcal{T}}$, and leading to approximation errors.

To overcome the aforementioned limitations, we propose to move beyond static representations and adopt a continuous, class-conditioned prior distribution $p(\hat{\boldsymbol{\phi}}_c \mid \boldsymbol{\theta})$, offering greater expressiveness and adaptability. This idea forms the foundation of our framework, **Global Variational Inference for Domain Adaptation (GVI-DA)**, which leverages variational inference [67], [84] to model class-level priors over a smooth latent space inferred directly from labeled source data.

By shifting from discrete anchor points to learned distributions, **GVI-DA** enables soft alignment of cross-domain features, reducing the projection gap while preserving semantic consistency. Mathematically, we reformulate the projection error as a variational optimization problem and demonstrate that our continuous formulation yields tighter bounds on training error compared to discrete priors. Moreover, while conventional variational approaches often assume a standard Gaussian prior $\mathcal{N}(0, \mathcal{I})$, such assumptions can hinder DA performance by neglecting task-specific structures. **GVI-DA** instead constructs its priors directly from the source data, capturing both class-conditional semantics and the geometric structure of the feature manifold. To ensure expressiveness and avoid posterior collapse, a common pitfall in multi-class variational models [1], [77], we introduce a global codebook learning mechanism coupled with randomized sampling. Additionally, to address the challenge of noisy pseudo-labels in the target domain, **GVI-DA** employs a generative augmentation strategy that selectively discards unreliable samples and regenerates robust target features guided by the learned global prior.

To summarize, this paper introduces a novel DA framework, *Global Variational Inference Enhanced Robust Domain Adaptation* (**GVI-DA**), as illustrated in Fig. 1. Our contributions are as follows:

- **Global continuous priors for DA.** To enable global knowledge-enhanced cross-domain decision making, we propose a novel DA method, **GVI-DA**. In contrast to prior global anchor-based approaches, GVI-DA constructs global continuous conditional priors from labeled source data, replacing rigid discrete distributions. This formulation not only promotes smoother cross-domain distribution alignment but also preserves intrinsic data structures through sample reconstruction driven by maximum likelihood estimation. Consequently, **GVI-DA** achieves tighter training error bounds and more reliable cross-domain optimization.
- **Codebook-driven latent modeling.** In **GVI-DA**, we leverage variational inference to replace the conventional $\mathcal{N}(0, \mathcal{I})$ prior with a continuous class-conditional distribution, aiming to better model cross-domain decision making. However, variational inference mechanisms are prone to *posterior collapse* in multi-class settings [1], [77]. To address this, we introduce a global codebook learning strategy combined with randomized sampling to promote latent diversity and effectively mitigate posterior collapse.
- **Generative augmentation for robust adaptation.** To mitigate negative transfer caused by noisy pseudo-labels, **GVI-DA** proposes a generative augmentation strategy. Specifically, high-entropy (low-confidence) pseudo-label samples are discarded to eliminate potential risks of negative transfer, while reliable target instances are regenerated through global prior-guided augmentation to enable robust cross-domain model training.
- **Extensive experiments and analysis.** We conducted extensive experiments on 27 image classification DA tasks across four benchmarks, demonstrating the superior performance of the proposed **GVI-DA** method over 38 state-of-the-art algorithms. We further provide in-depth insights into the effectiveness of continuous priors, codebook size sensitivity, robustness to target-domain pseudo-label noise, and computational efficiency, offering a deeper understanding of the proposed framework.

The remainder of this paper is organized as follows. Section II reviews related work. Section III details the proposed method. Section IV reports experimental results and analysis. Section V concludes the paper.

II. Related Work

Domain adaptation (DA) techniques can be broadly categorized into two paradigms based on their optimization frameworks: *shallow DA* and *deep DA*. Shallow DA methods, typically grounded in statistical alignment [45], [52], [51] or geometric regularization [50], [32], [39], enable global modeling of cross-domain data through closed-form analytical solutions or Rayleigh quotient optimization [74], [45]. However, such optimization routines often involve large-scale matrix computations across all samples, making them difficult to scale in massive dataset scenarios [60], [53]. In contrast, deep DA methods leverage the local sampling nature of batch learning and integrate end-to-end pipelines, allowing efficient multi-batch optimization for large-scale DA tasks. Nevertheless, this advantage comes at the cost of limited global modeling capability, as batch-based training inherently restricts the model's ability to capture global statistical and structural information across domains.

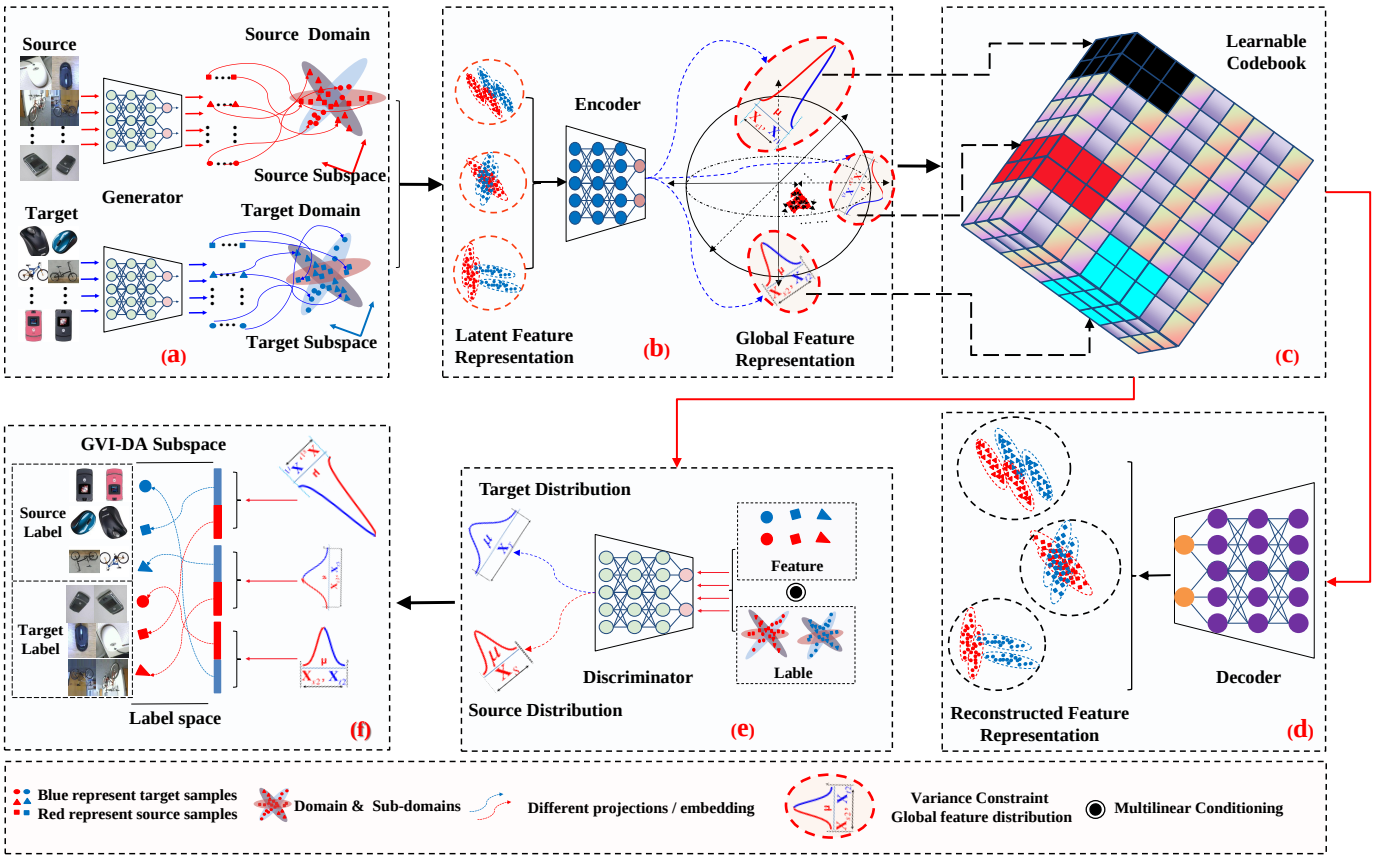

Fig. 1: Overview of the proposed **GVI-DA** framework. (a) Domain samples with class-specific geometry. (b) Global conditional distribution inference. (c) Codebook-based latent modeling to prevent posterior collapse. (d) Feature reconstruction regularization. (e) Conditional adversarial learning for joint distribution alignment. (f) Final classification results.

Building on this perspective, this section reviews three major categories of *deep DA* techniques: statistical alignment methods (Section II-A), adversarial learning methods (Section II-B), and generative model-based methods (Section II-C). We then discuss globally-aware DA approaches that aim to overcome the limitations of batch-wise optimization and analyze their inherent bottlenecks (Section II-D).

A. Statistic Matching-based DA (STA-DA)

The core idea of **STA-DA** is to integrate diverse statistical measurement strategies with deep learning-based optimization to facilitate cross-domain knowledge transfer. These methods typically employ statistical metrics, such as Wasserstein distance [66], frequency spectrum analysis [83], and Maximum Mean Discrepancy (MMD) [53], to quantify domain shift within kernel-induced feature spaces [56]. Meanwhile, by leveraging the nonlinear modeling capabilities and discriminative feature representations of deep networks (*e.g.*, ResNet [23], AlexNet [35]), STA-DA methods achieve robust and scalable domain alignment under complex real-world conditions. For example, the well-known **DAN** [43] mitigates marginal distribution divergence by incorporating a multi-kernel MMD loss into the fully connected layers of AlexNet. Building on **DAN**, **JAN** [48] jointly minimizes the divergence of both marginal and conditional distributions. **D-CORAL** [64] further extends this by introducing second-order statistics into the AlexNet [35] framework, which enhances the efficacy of the **DA** strategy. In contrast, more recent approaches such as **FDA** [83] and **MSDA** [22] present novel methods to reduce domain shift. **FDA** proposes using the low-frequency spectrum to measure dissimilarities across domains, while **MSDA** aligns cross-domains by minimizing the LAB color space representation. By swapping the content of low-frequency spectra [83] or LAB color space representations [22] between domains, these methods significantly mitigate domain shift.

The advantage of **STA-DA** lies in its flexibility to integrate various statistical metrics for optimizing domain discrepancy across kernel-induced feature spaces [51], typically formulated as $d(\mathcal{H}_{\mathcal{D}_\mathcal{S}}, \mathcal{H}_{\mathcal{D}_\mathcal{T}})$. However, its effectiveness heavily relies on the careful selection and tuning of statistical metrics and kernel hyperparameters. Additionally, **STA-DA** methods often suffer from limitations due to local batch sampling, which fails to reliably support global cross-domain statistical approximation required for robust decision boundaries. In contrast, our proposed **GVI-DA** enables explicit modeling of global knowledge.

B. Adversarial Loss-based DA

Adversarial learning-based DA methods leverage adversarial training [21] to align source and target domain features by making them indistinguishable through domain classifier training [7], [31]. Specifically, **DANN** [18] and **ADDA** [68]

TABLE I: Revisiting Enhanced Batch Learning for Globally-Aware Domain Adaptation.

Method	Anchor Constructed?	Anchor Update Strategy	Globally Learned?	Global Modeling Mechanism (Refined)	Reconstruction?
DSAN (2020) [92]	✗ No	N/A	✗ No	Class-weighted local alignment	✗ No
CAG-UDA (2019) [87]	✓ Yes (class-wise)	Per training stage	✗ No	Source anchor–guided pseudo-labeling	✗ No
MiRe (2022) [6]	✓ Yes (prototype)	EMA across batches	✓ Yes	Topology reasoning via anchor graph	✗ No
DRDA (2023) [28]	✓ Yes (global + local)	Batch-wise update	✓ Yes	Radial structure–aware alignment	✗ No
CMA (2024) [73]	✓ Yes (memory queue)	FIFO + sliding window	✓ Yes	Memory-based inter-domain aggregation	✗ No
TransVQA (2024) [65]	✓ Yes (implicit/codebook)	Learnable	✓ Yes	Codebook-based latent space alignment	✗ No
GAN-DA (2025) [53]	✓ Yes (predefined anchor)	Static + fusion	✓ Yes	Predefined anchor–conditioned alignment	✗ No
GVI-DA (2025)	✗ No (Inferred Distributions)	N/A	✓ Yes	Inferred Distributions + Coodbook	✓ Yes

learn domain-invariant feature subspaces by minimizing the divergence in marginal distributions. **MADA** [58] further improves alignment by using multiple domain discriminators, thereby aligning conditional data distributions. On the other hand, **DSN** [4] focuses on achieving domain-invariant representations by explicitly separating similarities and dissimilarities between the source and target domains. **GVB** [10] introduces a novel gradually vanishing bridge method that enhances feature representation by concurrently optimizing the generator and discriminator. **MADAN** [89] explores multi-source domain knowledge to tackle DA tasks. **CyCADA** [25] mitigates distribution divergence using a bi-directional GAN-based training framework.

Adversarial loss-based DA methods provide an intuitive and easily implementable framework for cross-domain alignment, contributing to their widespread adoption. However, due to their adversarial nature, these methods often suffer from unstable training and lack explicit guidance for likelihood-based distribution optimization [3], [82]. Typically, they minimize an adversarial objective $\mathcal{L}_{\text{adv}}$ to implicitly reduce domain divergence. Similar to statistic alignment-based DA methods, adversarial approaches focus on learning a discriminative mapping from input features to the label space, *i.e.*, $f_d(\mathbf{x};\theta) \mapsto \mathcal{P}(\mathbf{c})$, without explicitly modeling the data distribution $\mathcal{P}(\mathbf{x})$. In contrast, the proposed **GVI-DA** leverages a variational inference framework to jointly model data and label distributions, enabling globally aligned cross-domain conditional inference. This design facilitates robust and semantically coherent latent representations, offering a principled alternative to the limitations of purely adversarial alignment methods.

C. Generative Model-based DA

In contrast to discriminative model-based DA methods that focus on learning the conditional distribution $f_d(\mathbf{x};\theta) \mapsto \mathcal{P}(\mathbf{c} \mid \mathbf{x})$, generative model-based DA methods aim to model the full joint distribution $\mathcal{P}(\mathbf{x},\mathbf{c})$ by simultaneously capturing both data and label spaces, *i.e.*, $f_g(\mathbf{x};\theta) \mapsto \mathcal{P}(\mathbf{x},\mathbf{c})$. Such approaches [82], [30] enhance DA by preserving semantically meaningful structures in the learned latent space, thereby reducing overfitting and improving generalization.

For example, Zhang *et al.* [86] formulated DA as a Bayesian inference problem within a probabilistic graphical model framework. Building upon this, **VDI** [80] introduced domain indices into a variational Bayesian framework to handle multi-domain data. Recently, diffusion generative models [63], [24], [40], based on Markovian sequential optimization, have emerged as a promising paradigm for DA by refining the joint probability distribution $\mathcal{P}_\theta(\mathbf{x}_\mathcal{T}, \mathbf{x}_\mathcal{S})$ through reverse diffusion, facilitating smooth domain transitions and robust alignment. **DAD** [59] bridges source and target domains by simulating a sequence of distributions with minimal discrepancies between adjacent steps, achieving seamless cross-domain blending. **Trans-Diff** [33] introduces cross-domain prompts to generate semantically-aware pseudo-target domain images, significantly improving DA performance. **DDA** [19] employs diffusion models to align data structures within noisy latent spaces, reducing domain divergence. Furthermore, Kamil *et al.* [12] enhance classifier guidance to improve conditional distribution-aware adaptation, while Prof. Li *et al.* [17] further refine cross-domain alignment through diffusion-based purification of target domain labels.

With the rapid advancement of generative models, DA methods built upon generative frameworks have garnered increasing attention for their potential to address cross-domain decision tasks. In particular, diffusion-based approaches offer a promising bridge between theoretical modeling and practical DA applications. For instance, **DDBM** [91] adopts an interpolation-based strategy to jointly transfer style and content within the original feature space, while the Schrödinger diffusion bridge [11] enables bidirectional optimization between source and target domains. These methods demonstrate strong potential for addressing fundamental challenges in DA. However, generative DA remains limited by substantial computational overhead and relatively weak discriminative capability for label inference. Moreover, in comparison to the proposed **GVI-DA**, batch-level inconsistencies in generative pipelines still hinder stable cross-domain alignment. Overcoming these limitations is essential for developing globally informed, decision-aware generative DA frameworks as the proposed **GVI-DA** does.

D. Revisiting Batch Learning for Globally-Aware DA

All the aforementioned methods fall under the umbrella of deep learning-based DA. However, they inherently suffer from limitations imposed by batch-wise sampling, which constrains global structure modeling. To address this, prior studies have explored enhancing batch learning mechanisms to alleviate the issue. As summarized in Table I, **DSAN** [92] tackles class-level distribution mismatch by performing class-weighted alignment within individual batches, yet it lacks global semantic awareness. To mitigate this, a series of anchor-based methods have emerged to enhance global conditional distribution guidance. **CAG-UDA** [87] constructs class-wise anchors from the source domain during training. However, these anchors only encode source-to-target constraints and may neglect target semantics, limiting cross-domain awareness. **MiRe** [6] and

DRDA [28] further enhance global modeling through topological and radial constraints, respectively, but their anchors remain constrained by batch-level sampling, making them susceptible to inter-batch inconsistencies. **CMA** [73] extends batch statistics via FIFO-based memory queues to enlarge the temporal batch window, however, its global modeling capacity remains tightly coupled to memory size and update dynamics. In contrast, **TransVQA** [65] foregoes explicit anchors by projecting source and target samples into a shared codebook space for implicit alignment, though domain-specific activations in different codebook regions may still lead to semantic drift. The recent proposed **GAN-DA** [53] eliminates reliance on batch sampling by introducing a globally shared prior anchor space, termed *Predefined Feature Representation (PFR)*, enabling domain-shared semantics and domain-specific variations to be aligned within a unified latent space.

However, existing global anchor-based DA methods often struggle to unify cross-domain distributions smoothly due to the limitations of discrete prior modeling, which frequently leads to suboptimal approximation and increased training error. In contrast, as summarized in Table I, the proposed **GVI-DA** leverages a variational inference framework to construct continuous, learnable class-conditional priors that replace sparse, discrete anchor distributions. This formulation enables smoother distribution alignment and tighter control of the training error bound. To further mitigate the risk of posterior collapse [1], [77] during prior learning, **GVI-DA** incorporates a global codebook learning mechanism combined with randomized sampling, which encourages diversity and expressiveness in the latent representations. Additionally, to address the challenge of negative transfer caused by noisy pseudo-labels in the target domain, **GVI-DA** adopts a generative augmentation strategy that filters out high-entropy (*i.e.*, low-confidence) samples and regenerates reliable target instances guided by the learned global prior. This design improves training stability and ensures sufficient target-domain supervision for robust domain adaptation.

III. THE PROPOSED METHOD

We begin by introducing the notations utilized throughout this paper, as detailed in Sect.III-A. In Sect.III-B, we present a comprehensive, step-by-step breakdown of the proposed **GVI-DA** approach. Finally, in Sect.III-C, we provide an in-depth discussion of the rationale behind the overall optimization strategy employed within the **GVI-DA** model to achieve efficient cross-domain classification.

A. Notations and Problem Statement

We use the calligraphic symbols $\mathcal{S}$ and $\mathcal{T}$ to denote the *source* and *target* domains, respectively. Bold uppercase letters (*e.g.*, $\mathbf{M} = (m_{ij})$) denote matrices, where $\mathbf{m}^i$ is the i-th row and $\mathbf{m}_j$ is the j-th column. Bold lowercase letters (*e.g.*, $\mathbf{x}$) represent vectors. A domain $\mathcal{D}$ is defined as a pair of an ℓ-dimensional feature space $\mathcal{X}$ and a marginal distribution $\mathcal{P}(\mathbf{x})$, *i.e.*, $\mathcal{D} = \{\mathcal{X}, \mathcal{P}(\mathbf{x})\}$ with $\mathbf{x} \in \mathcal{X}$. Given a domain $\mathcal{D}$, a task $\mathcal{TK}$ consists of a label space $\mathcal{Y}$ of size C and a classifier $f(\mathbf{x})$, *i.e.*, $\mathcal{TK} = \{\mathcal{Y}, f(\mathbf{x})\}$, where $f(\mathbf{x}) = \mathcal{Q}(y \mid \mathbf{x})$ models the class-conditional distribution over $\mathcal{Y}$. In unsupervised domain adaptation (UDA), we are given a labeled source domain $\mathcal{D}_\mathcal{S} = \{\mathbf{x}_\mathcal{S}^i, \mathbf{y}_\mathcal{S}^i\}_{i=1}^{n_\mathcal{S}}$, where $\mathbf{X}_\mathcal{S} = [\mathbf{x}_\mathcal{S}^1, \ldots, \mathbf{x}_\mathcal{S}^{n_\mathcal{S}}]$ and $\mathbf{Y}_\mathcal{S} = [\mathbf{y}_\mathcal{S}^1, \ldots, \mathbf{y}_\mathcal{S}^{n_\mathcal{S}}]^\top \in \mathbb{R}^{n_\mathcal{S} \times C}$ denote the source data and labels. The unlabeled target domain is defined as $\mathcal{D}_\mathcal{T} = \{\mathbf{x}_\mathcal{T}^j\}_{j=1}^{n_\mathcal{T}}$, where $\mathbf{X}_\mathcal{T} = [\mathbf{x}_\mathcal{T}^1, \ldots, \mathbf{x}_\mathcal{T}^{n_\mathcal{T}}]$ and $\mathbf{Y}_\mathcal{T} = [\mathbf{y}_\mathcal{T}^1, \ldots, \mathbf{y}_\mathcal{T}^{n_\mathcal{T}}]^\top \in \mathbb{R}^{n_\mathcal{T} \times C}$ are the target data and their (unobserved) labels. Although the feature and label spaces are shared across domains ($\mathcal{X}_\mathcal{S} = \mathcal{X}_\mathcal{T}$, $\mathcal{Y}_\mathcal{S} = \mathcal{Y}_\mathcal{T}$), the marginal and conditional distributions differ, i.e., $\mathcal{P}(\mathcal{X}_\mathcal{S}) \neq \mathcal{P}(\mathcal{X}_\mathcal{T})$ and $\mathcal{Q}(\mathcal{Y}_\mathcal{S} \mid \mathcal{X}_\mathcal{S}) \neq \mathcal{Q}(\mathcal{Y}_\mathcal{T} \mid \mathcal{X}_\mathcal{T})$. A class-specific subdomain in the source domain is denoted as $\mathcal{D}_\mathcal{S}^{(c)} = \{\mathbf{x}_\mathcal{S}^i \in \mathbf{X}_\mathcal{S} \mid \mathbf{y}_\mathcal{S}^i = c\}$. Correspondingly, target subdomains $\mathcal{D}_\mathcal{T}^{(c)}$ are constructed by assigning pseudo-labels to $\mathbf{X}_\mathcal{T}$ via a source-trained base classifier.

B. Formulation

According to the theoretical error bound formalized in Eq.(1), the proposed **GVI-DA** progressively optimizes each term as follows. First, Section.III-B1 adopts Source Domain Structural Risk Minimization (**SRM**) [71] to explicitly reduce the source-domain classification error, addressing **Term.1**. Subsequently, Section.III-B2 introduces a global variational inference framework to smoothly align cross-domain conditional distributions with narrowed continuous priors while preserving intrinsic data structures, thereby optimizing **Term.2** and **Term.3**. To further mitigate the risk of posterior collapse under variance constraints, Section.III-B3 incorporates global codebook learning and randomized sampling strategies. Moreover, Section.III-B4 proposes a pseudo-label filtering and sample regeneration mechanism to combat negative transfer caused by noisy target pseudo-labels. Finally, Section.III-B5 introduces a conditional adversarial optimization strategy to explicitly align joint sample-label distributions, enhancing discriminative and reliable cross-domain decision boundaries.

1) Structural Risk Minimization for the Source Domain: As shown in Fig.1(a), our framework begins by minimizing **Term.1** in Eq.(1), which corresponds to structural risk minimization on the source domain. This step involves training a source-domain classifier in a fully supervised manner. Based on a feature generator $\mathcal{G}$, we define the hypothesis $\mathcal{F}_\mathcal{S} : \mathcal{F}_\mathcal{S}(\mathcal{G}(\mathcal{X}_\mathcal{S})) \to \mathcal{Y}_\mathcal{S}$, which maps source-domain inputs to their corresponding labels. The overall objective can be formalized as:

$$\mathcal{F}_\mathcal{S} = \arg\min_{\mathcal{F}_\mathcal{S} \in \mathcal{H}_\mathcal{K}} \mathbb{E}_{(x_\mathcal{S}, y_\mathcal{S}) \sim \mathcal{D}_\mathcal{S}} \Big[l(\mathcal{F}_\mathcal{S}(\mathcal{G}(x_\mathcal{S})), y_\mathcal{S}) \Big] + \mathcal{R}(\mathcal{F}_\mathcal{S}). \quad (2)$$

Here, the loss function $l(\cdot)$ ensures accurate label prediction on the source domain, while the regularization term $\mathcal{R}(\mathcal{F}_\mathcal{S})$ constrains the capacity of the hypothesis space $\mathcal{H}_\mathcal{K}$ to prevent model overfitting.

Although the above optimization partially minimizes the theoretical error bound for DA, residual domain shift still impedes reliable functional mapping in the target domain, *i.e.*, $\mathcal{F}_\mathcal{S}(\mathcal{G}(\mathcal{X}_\mathcal{T})) \neq \mathcal{Y}_\mathcal{T}$. This misalignment is primarily due to divergence between the source and target labeling functions, expressed as $\mathrm{div}(\mathcal{F}_\mathcal{S}, \mathcal{F}_\mathcal{T})$, which directly hinders the minimization of **Term.3** in Eq. (1). The underlying causes of this divergence can be attributed to two key factors:

- ***Cross-Domain Distribution Shift:*** The divergence between cross-domain conditional distributions, *i.e.*, $\mathcal{Q}(\mathbf{y}_{\mathcal{S}} \mid \mathbf{x}_{\mathcal{S}}) \neq \mathcal{Q}(\mathbf{y}_{\mathcal{T}} \mid \mathbf{x}_{\mathcal{T}})$, hinders knowledge transfer and impedes unified cross-domain decision making.
- ***Pseudo-Label Noise in the Target Domain:*** The existing *distribution shift* inevitably introduces errors into the pseudo-labeled target samples, steering the model optimization toward a suboptimal classifier $\mathcal{F}'_{\mathcal{T}}$ rather than the true target-domain classifier $\mathcal{F}_{\mathcal{T}}$. Consequently, unifying the cross-domain labeling functions is formulated as: $\text{div}(\mathcal{F}_{\mathcal{S}}, \mathcal{F}_{\mathcal{T}}) = \text{div}(\mathcal{F}_{\mathcal{S}}, \mathcal{F}'_{\mathcal{T}}) + \text{div}(\mathcal{F}'_{\mathcal{T}}, \mathcal{F}_{\mathcal{T}})$, where the additional discrepancy $\text{div}(\mathcal{F}'_{\mathcal{T}}, \mathcal{F}_{\mathcal{T}})$ introduces extra training error, degrading the approximation of the cross-domain decision boundary.

To address the *cross-domain distribution shift*, Section.III-B2 introduces a variational inference strategy that enhances global knowledge awareness and aligns cross-domain conditional distributions, thereby optimizing **Term.2** in Eq. (1). To mitigate the *Pseudo-Label Noise in the Target Domain*, Section.III-B4 proposes an entropy-based filtering strategy to discard low-confidence pseudo-labeled samples. Simultaneously, a generative augmentation mechanism is employed to synthesize reliable target samples, thereby improving the robustness of cross-domain decision making.

As illustrated in Fig. 2, the left part depicts the principle of anchor-based DA, which aligns cross-domain conditional distributions using fixed class-wise anchors. In contrast, the right part highlights the global inference strategy of **GVI-DA**, which embeds both source and target samples into a shared, continuous, class-conditional latent space.

2) Globally Informed Cross-Domain Distribution Alignment: Previous studies [51], [50] have shown that effective cross-domain alignment requires minimizing two types of distributional discrepancy: marginal distribution shift and conditional distribution divergence. Formally, they are defined as $\text{div}_{\text{marg}} = \|\mathcal{P}(\mathcal{X}_{\mathcal{S}}) - \mathcal{P}(\mathcal{X}_{\mathcal{T}})\|$, $\text{div}_{\text{condi}} = \|\mathcal{Q}(\mathcal{Y}_{\mathcal{S}} \mid \mathcal{X}_{\mathcal{S}}) - \mathcal{Q}(\mathcal{Y}_{\mathcal{T}} \mid \mathcal{X}_{\mathcal{T}})\|$. We demonstrate in the following lemma that under the standard unsupervised domain adaptation (UDA) setting, where the source and target domains share an identical label space, aligning the conditional distributions is sufficient to guarantee marginal alignment.

Lemma III.1. *if* $div_{condi} \to 0$*, then* $div_{marg} \to 0$*.*

Proof. In practical optimization, the divergence of conditional distributions is typically approximated by comparing class-conditional sample distributions:

$$\text{div}_{\text{condi}} \approx \|\mathcal{Q}(\mathcal{X}_{\mathcal{S}} \mid \mathcal{Y}_{\mathcal{S}}) - \mathcal{Q}(\mathcal{X}_{\mathcal{T}} \mid \mathcal{Y}_{\mathcal{T}})\|.$$

Assuming the conditional distributions are perfectly aligned, we have

$$\mathcal{Q}(\mathcal{X}_{\mathcal{S}} \mid \mathcal{Y}_{\mathcal{S}}) = \mathcal{Q}(\mathcal{X}_{\mathcal{T}} \mid \mathcal{Y}_{\mathcal{T}}).$$

Integrating both sides over the shared label space yields

$$\int \mathcal{Q}(\mathcal{X}_{\mathcal{S}} \mid \mathcal{Y}_{\mathcal{S}})\, d\mathcal{Y}_{\mathcal{S}} = \int \mathcal{Q}(\mathcal{X}_{\mathcal{T}} \mid \mathcal{Y}_{\mathcal{T}})\, d\mathcal{Y}_{\mathcal{T}}.$$

Since the source and target domains share an identical label space under the UDA setting, this implies $\mathcal{Q}(\mathcal{X}_{\mathcal{S}}, \mathcal{Y}_{\mathcal{S}}) = \mathcal{Q}(\mathcal{X}_{\mathcal{T}}, \mathcal{Y}_{\mathcal{T}})$, which further leads to $\mathcal{P}(\mathcal{X}_{\mathcal{S}}) = \mathcal{P}(\mathcal{X}_{\mathcal{T}})$. □

Therefore, aligning conditional distributions inherently results in the alignment of marginal distributions. Based on this observation, we introduce a *Global Variational Inference* (**GVI**) mechanism that aligns cross-domain conditional distributions from a global perspective, serving as a principled approach to mitigate domain shift.

Global Variational Inference mechanism Motivated Cross-domain Conditional Distribution Alignment:

To address conditional distribution alignment, the proposed **GVI** mechanism is broadly divided into the following two steps:

Step 1. ***Modeling the Continuous Prior Feature Distribution.*** To overcome the limitations of discrete priors in anchor-based DA methods as discussed in Section II-D, a *Continuous Prior Feature Distribution* is introduced to enable more flexible and expressive global alignment.

a) Motivation: As illustrated in the left of Fig. 2, anchor-based DA methods rigidly project both source and target feature distributions, $\mathcal{P}(\mathcal{G}(x))_{x \in \mathcal{D}_{\mathcal{S}}^{(c)}}$ and $\mathcal{P}(\mathcal{G}(x))_{x \in \mathcal{D}_{\mathcal{T}}^{(c)}}$, onto a fixed anchor $\mathbf{ACH}_c$, inducing a multi-to-one approximation. This rigid mapping results in nonzero approximation error:

$$\inf_{\mathbf{PFR}_c} \mathbb{E}_{\mathbf{z} \sim \mathcal{P}(\mathcal{G}(x))_{x \in \mathcal{D}_{\mathcal{S}}^{(c)} \cup \mathcal{D}_{\mathcal{T}}^{(c)}}} [\|\mathbf{z} - \mathbf{ACH}_c\|] > 0, \quad (3)$$

whenever the distribution is continuous and non-degenerate. Let μ denote the continuous probability measure of cross-domain features, and $\delta(\mathbf{ACH}_c)$ the Dirac measure at anchor $\mathbf{ACH}_c$. As $\delta(\mathbf{ACH}_c)$ assigns all mass to a single point, it cannot support the continuous domain of μ, yielding nonzero divergence [5], *i.e.*, $\|\mu - \delta(\mathbf{ACH}_c)\| > 0$. This exposes a core limitation of discrete anchors: their inability to model distributional continuity leads to approximation error and training instability.

b) Implementation: To overcome this issue, we replace the discrete anchor $\mathbf{ACH}_c$ with a continuous class-wise Gaussian prior $\mathbf{PFD}_c \sim \mathcal{N}(\mu_c, \Sigma_c)$, which serves as a global reference for aligning source and target samples in class c. The alignment challenge then becomes measuring consistency between batch-sampled sub-domains and this global prior. As shown in the right of Fig. 2, instead of point-matching via MMD, we use an encoder $\mathbf{E}$ to estimate empirical batch distributions $\mathcal{P}_{\text{batch}}(\mathbf{E}(\mathcal{G}(x)))_{x \in \mathcal{D}_{\mathcal{S}}^{(c)}}$ and $\mathcal{P}_{\text{batch}}(\mathbf{E}(\mathcal{G}(x)))_{x \in \mathcal{D}_{\mathcal{T}}^{(c)}}$ [55]. The alignment objective becomes minimizing the KL divergence between the empirical and prior distributions:

$$\min \textstyle\sum_{i=1}^{C} D_{\text{KL}} \left(\mathcal{P}_{\text{batch}}(\mathbf{E}(\mathcal{G}(x)))_{x \in \mathcal{D}_{\mathcal{S}}^{(i)} \cup \mathcal{D}_{\mathcal{T}}^{(i)}} \parallel \mathbf{PFD}_i \right). \quad (4)$$

This distribution-to-distribution alignment mitigates batch-wise statistical inconsistencies and provides a principled solution to the non-equilibrium issue, enabling globally consistent conditional alignment.

Step 2. ***Alignment aware of Intrinsic Cross-Subdomain Distribution*** To further reduce approximation errors introduced by predefined global priors, we enhance the alignment

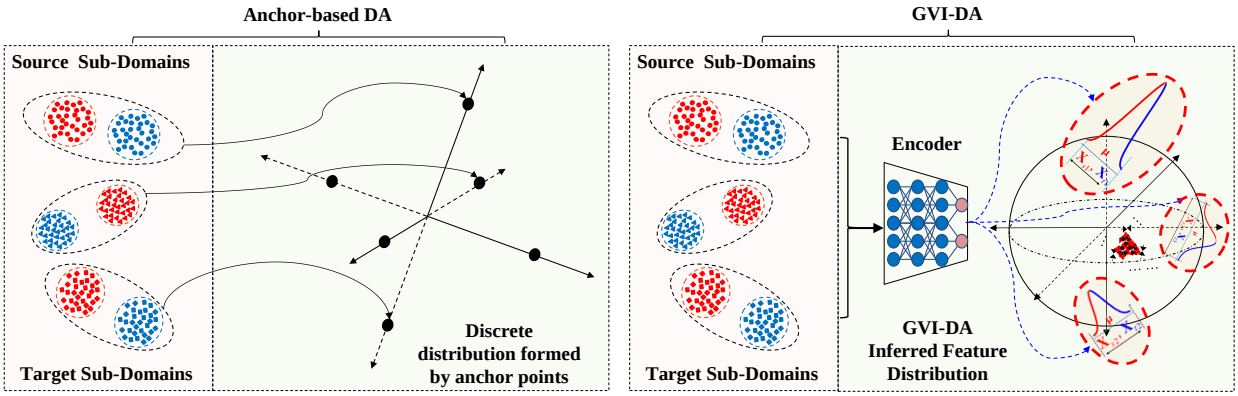

Fig. 2: The left part depicts the principle of anchor-based DA, which aligns cross-domain conditional distributions using fixed class-wise anchors. In contrast, the right part highlights the global inference strategy of **GVI-DA**, which embeds both source and target samples into a shared, continuous, class-conditional latent distribution.

process by explicitly incorporating the intrinsic structure of source and target sub-domain distributions.

a) Motivation: Although the KL-based alignment in Eq. (4) enables batch-to-prior matching, the handcrafted prior $\mathbf{PFD}_c$ may not accurately reflect the true sub-domain distributions $\mathcal{P}\big(\mathbf{E}(\mathcal{G}(x))\big)_{x\in\mathcal{D}_{\mathcal{S}}^{(c)}}$ and $\mathcal{P}\big(\mathbf{E}(\mathcal{G}(x))\big)_{x\in\mathcal{D}_{\mathcal{T}}^{(c)}}$, leading to a non-negligible training error lower bound:

$$\inf_{\mathbf{PFD}\in\mathcal{D}} \mathrm{Div}\big(\mathcal{P}(\mathbf{E}(\mathcal{G}(x)))\,\big\|\,\mathbf{PFD}\big) \geq \epsilon_{\text{train}} > 0, \quad (5)$$

where ϵ_{train} reflects the irreducible error from prior-subdomain mismatch. In addition, the variational inference framework adopted in the proposed **GVI-DA**, commonly relies on a mean-field approximation [88], [69] that factorizes the latent prior:

$$p(\mathbf{PFD}) = \textstyle\prod_{i=1}^{d} p(PFD_i), \quad \text{or equivalently, } \Sigma = \mathrm{diag}(\sigma^2,\ldots,\sigma^2), \quad (6)$$

which simplifies computation but ignores inter-dimensional correlations and semantic structure, ultimately limiting the alignment fidelity of the global prior.

b) Implementation: To overcome the limitations of predefined priors and better reflect the intrinsic cross-subdomain distributions, we reformulate the global prior $\mathbf{PFD}_c$ as a data-driven class-conditional distribution constructed from source-domain features. Specifically, instead of arbitrarily setting $\mathbf{PFD}_c$, we define it as the empirical source-domain feature distribution aggregated over an epoch: $\mathbf{PFD}_c \leftarrow \mathcal{P}_{\text{epoch}}\big(\mathcal{G}(x)\big)_{x\in\mathcal{D}_{\mathcal{S}}^{(c)}}$, which captures stable, class-specific statistics from real data. The alignment objective in Eq. (4) is then revised as:

$$\min \textstyle\sum_{i=1}^{C} D_{\text{KL}}\Big(\mathcal{P}_{\text{batch}}\big(\mathbf{E}(\mathcal{G}(x))\big)_{x\in\mathcal{D}_{\mathcal{S}}^{(i)}\cup\mathcal{D}_{\mathcal{T}}^{(i)}}\,\Big\|\,\mathcal{P}_{\text{epoch}}\big(\mathcal{G}(x)\big)_{x\in\mathcal{D}_{\mathcal{S}}^{(i)}}\Big). \quad (7)$$

This distribution-to-distribution KL minimization effectively mitigates batch-level inconsistencies and supports stable global alignment. Importantly, the epoch-level source prior evolves with training and dynamically encodes class-conditional structure aligned with encoder updates. Furthermore, each class-wise prior models dimension-specific statistics as $\mathcal{N}(\mu_c^i, \sigma_c^i)$, preserving feature-wise variability and addressing the limitations of mean-field assumptions. This formulation enables semantically-aware, globally consistent domain adaptation.

In summary, minimizing Eq.(7) enforces global conditional alignment and optimizes **Term.2** in Eq.(1). However, as it focuses on distribution matching, Eq.(7) does not directly support decision boundary refinement which is essential for minimizing **Term.3**. To this end, we introduce a variance-constrained mechanism that promotes compact and class-separable features, facilitating reliable labeling and tighter error bounds.

Variance-Constrained Mechanism for Optimizing Cross-Domain Labeling Functions:

Following Eq. (7), the ideal objective is to align each cross-domain sub-distribution with its corresponding global class-conditional prior $\mathcal{P}_{\text{epoch}}\big(\mathcal{G}(x)\big)_{x\in\mathcal{D}_{\mathcal{S}}^{(i)}}$. To further promote *cross-domain decision boundary optimization*, we introduce a variance-constrained mechanism inspired by the margin-based principle of support vector machines (SVM) [9], encouraging larger inter-class separability in the latent space. Specifically, we minimize the overlap between any pair of class-conditional priors:

$$\int \min\Big(\mathcal{P}_{\text{epoch}}^{(i)}(\mathbf{z}), \mathcal{P}_{\text{epoch}}^{(j)}(\mathbf{z})\Big) d\mathbf{z} \approx 0 \quad (\forall\, i \neq j), \quad (8)$$

which encourages decision boundaries to pass through low-density regions. Practically, we assume each prior $\mathcal{P}_{\text{epoch}}\big(\mathcal{G}(x)\big)_{x\in\mathcal{D}_{\mathcal{S}}^{(i)}}$ follows a Gaussian distribution. The mean $\boldsymbol{\mu}_i$ is computed from all class-i source features in an epoch, while the covariance is set to an isotropic matrix scaled by $1/C$, reflecting the intuition that more classes require tighter variance control for separability: $\mathcal{P}_{\text{epoch}}\big(\mathcal{G}(x)\big)_{x\in\mathcal{D}_{\mathcal{S}}^{(i)}} \sim \mathcal{N}\left(\boldsymbol{\mu}_i, \frac{1}{C}\mathbf{I}\right)$. Accordingly, the KL-based alignment in Eq. (7) is updated as:

$$\begin{aligned} &\min \sum_{i=1}^{C} D_{\text{KL}}\Big(\mathcal{P}_{batch}\big(\mathbf{E}(\mathcal{G}(x))\big)_{x\in\mathcal{D}_{\mathcal{S}}^{(i)}\cup\mathcal{D}_{\mathcal{T}}^{(i)}}\,\Big\|\,\mathcal{P}_{\text{epoch}}\big(\mathcal{G}(x)\big)_{x\in\mathcal{D}_{\mathcal{S}}^{(i)}}\Big) \\ &\text{s.t.}\ \ \mathcal{P}_{\text{epoch}}\big(\mathcal{G}(x)\big)_{x\in\mathcal{D}_{\mathcal{S}}^{(i)}} \sim \mathcal{N}\Big(\boldsymbol{\mu}_i, \tfrac{1}{C}\mathbf{I}\Big)_{x\in\mathcal{D}_{\mathcal{S}}^{(i)}} \end{aligned} \quad (9)$$

This formulation not only aligns mini-batch distributions with global class-aware priors but also regularizes intra-class variance, facilitating the learning of more discriminative and stable cross-domain decision boundaries.

However, while the variance-constrained mechanism in Eq. (9) effectively promotes inter-class separation and facilitates decision boundary optimization, it also exacerbates the risk of *posterior collapse* [1], [77], particularly in large-scale

classification tasks. As the number of categories C increases, the fixed class-wise prior variance $\frac{1}{C}$ diminishes, leading to the limiting behavior:

$$\lim_{C\to large} \tfrac{1}{C} \to 0 \Rightarrow \mathbf{PFD}_c \sim \mathcal{N}(\boldsymbol{\mu}_c, \tfrac{1}{C}\mathbf{I}) \to \delta(\boldsymbol{\mu}_c), \quad (10)$$

where $\delta(\boldsymbol{\mu}_c)$ denotes a Dirac delta centered at $\boldsymbol{\mu}_c$, representing a collapsed distribution with vanishing variance. This excessive compression undermines semantic diversity in the latent space and restricts the encoder's capacity to capture meaningful variations. Consequently, the latent matching objective in Eq. (9) could become ineffective, as the collapsed distributions fail to provide sufficient latent embedding capacity for large-scale DA tasks, ultimately hindering the reduction of the training error bound. To address this issue, we propose in Section III-B3 a *Global Codebook Inference with Randomized Sampling* strategy to mitigate the risk of posterior collapse.

3) Global Codebook Inference with Randomized Sampling for Mitigating Posterior Collapse: To address the risk of *posterior collapse* in probabilistic inference models, a natural solution is the *Vector Quantized Variational Autoencoder (VQ-VAE)* [70], which replaces the continuous mean-field prior in VAEs (i.e., $\mathcal{N}(0, I)$) with a learnable discrete codebook. This design avoids the over-concentration of latent representations by enforcing discrete, sample-dependent assignments, thereby promoting more stable and informative embeddings. The standard VQ-VAE optimization objective is defined as:

$$L = \log p(x \mid z_q(x)) + \|\,\mathrm{sg}[z_{en}(x)] - e\|_2^2 + \beta\|z_{en}(x) - \mathrm{sg}[e]\|_2^2, \quad (11)$$

where $z_{en}(x)$ is the encoder output and e is the nearest codebook entry. The second term encourages the encoder to match the selected codeword (with gradients detached via $\mathrm{sg}[\cdot]$), while the third term updates the codebook toward the encoder output. Together, these terms maintain diverse, sample-specific associations and prevent latent collapse. Building on this framework, we define a discrete codebook $\mathcal{E} = \{e_k\}_{k=1}^K$. Following the variance-constrained setup in Eq. (9), each latent feature $\mathbf{E}(\mathcal{G}(x))$ is quantized to its nearest codeword:

$$\begin{aligned} &z_q(x) = \arg\min_{e_k\in\mathcal{E}} \|\mathbf{E}(\mathcal{G}(x)) - e_k\|_2^2 \ . \\ &\text{s.t.} \ \ \mathcal{P}_{\text{epoch}}\big(\mathcal{G}(x)\big)_{x\in\mathcal{D}_{\mathcal{S}}^{(i)}} \sim \mathcal{N}\Big(\boldsymbol{\mu}_i, \tfrac{1}{C}\mathbf{I}\Big)_{x\in\mathcal{D}_{\mathcal{S}}^{(i)}} \end{aligned} \quad (12)$$

However, as the number of categories C increases (e.g., C=65 in Office-Home [72], C=345 in DomainNet [60]), the fixed prior variance $\frac{1}{C}$ diminishes, resulting in the limiting behavior: $\lim_{C\to large} \frac{1}{C} \to 0 \Rightarrow \mathcal{P}_{\text{epoch}}\big(\mathcal{G}(x)\big) \to \delta(\boldsymbol{\mu}_i)$, where $\delta(\boldsymbol{\mu}_i)$ denotes a near-point mass centered at $\boldsymbol{\mu}_i$. Under such constraints, even within VQ-VAE, the compressed latent space can induce extreme quantization, mapping all samples in class i to the same code: $\forall\, x, x' \in \mathcal{D}_{\mathcal{S}}^{(i)}, \quad z_q(x) = z_q(x')$, thereby reintroducing *posterior collapse* in the discrete latent space. This severely limits feature diversity and compromises the expressiveness of learned representations. To address this, we introduce two complementary strategies (illustrated in Fig. 3): *Global Codebook Inference* (Fig. 3(b)) and *Randomized Sampling* (Fig. 3(c)). These enhancements jointly promote latent diversity and stability, effectively mitigating posterior collapse and improving the model's capacity to capture complex cross-domain semantics.

Global Codebook Learning for Cross-domain Samples Inference:

To prevent the collapse of same-class samples onto a single dictionary element under extreme latent space compression, as discussed in Eq. (12), we propose a *Global Codebook Learning* mechanism. As illustrated in Fig. 3(b), each cross-domain sample interacts with a global codebook $\mathcal{E} = \{e_k\}_{k=1}^K$, where each codeword $e_k \in \mathbb{R}^d$ shares the same dimensionality as the encoded features $\mathbf{E}(\mathcal{G}(x))_{x\in\mathcal{D}_{\mathcal{S}}^{(i)}\cup\mathcal{D}_{\mathcal{T}}^{(i)}}$. Instead of hard nearest-neighbor assignments as in VQ-VAE, we adopt a *probabilistic soft assignment* strategy:

$$P\big(e_k \mid \mathbf{E}(\mathcal{G}(x))\big) = \frac{\exp\big(-d(\mathbf{E}(\mathcal{G}(x)), e_k)\big)}{\sum_{j=1}^K \exp\big(-d(\mathbf{E}(\mathcal{G}(x)), e_j)\big)}, \quad (13)$$

where $d(\cdot,\cdot)$ denotes a distance metric (e.g., cosine or Euclidean distance). This design encourages each sample to interact with multiple codewords, enhancing latent diversity and mitigating collapse. To further prevent dominance by a single dictionary element, particularly under variance-constrained settings, we introduce an *entropy maximization* objective:

$$\begin{aligned} &\max\ H\big(P\big(e_k \mid \mathbf{E}(\mathcal{G}(x))\big)\big) = \\ &-\textstyle\sum_{k=1}^K P\big(e_k \mid \mathbf{E}(\mathcal{G}(x))\big)\ \log\ P\big(e_k \mid \mathbf{E}(\mathcal{G}(x))\big), \end{aligned} \quad (14)$$

which promotes diverse utilization of codebook entries and prevents premature saturation. Nonetheless, a critical question arises: *under the extreme variance constraints imposed by Eq. (12), particularly in large-category DA tasks, does latent compression cause uniform interaction weights between samples and codewords?* If so, even though samples are associated with different dictionary elements, they could share similar association patterns, thereby reintroducing *posterior collapse*. To address this, we propose a *Randomized Sampling* mechanism, which further enhances the diversity and adaptability of latent-to-codeword assignments.

Randomized Sampling for Dynamic Codebook Association:

To overcome the extreme *posterior collapse* induced by variance constraints in Eq. (12), we propose a *Randomized Sampling* mechanism to enhance sample-level stochasticity within the codebook learning paradigm. Specifically, instead of deterministically optimizing based on the top-ranked dictionary entries in Eq. (13), we adopt a Gumbel-Softmax sampling strategy [29] to enable stochastic assignments across multiple codewords. Given the soft assignment probabilities in Eq. (13), we introduce Gumbel noise $g_k = -\log(-\log(u_k))$, where $u_k \sim \mathrm{Uniform}(0,1)$, to inject randomness into the selection process. The randomized assignment is then computed as:

$$\tilde{P}\big(e_k \mid \mathbf{E}(\mathcal{G}(x))\big) = \frac{\exp\big((\log P(e_k|\mathbf{E}(\mathcal{G}(x))) + g_k)/\tau\big)}{\sum_{j=1}^K \exp\big((\log P(e_j|\mathbf{E}(\mathcal{G}(x))) + g_j)/\tau\big)}, \quad (15)$$

where τ is a temperature parameter that controls the smoothness of the sampling distribution. This stochastic formulation allows each sample to dynamically explore a wider range of dictionary entries during training, effectively avoiding fixed and overly confident associations. As illustrated

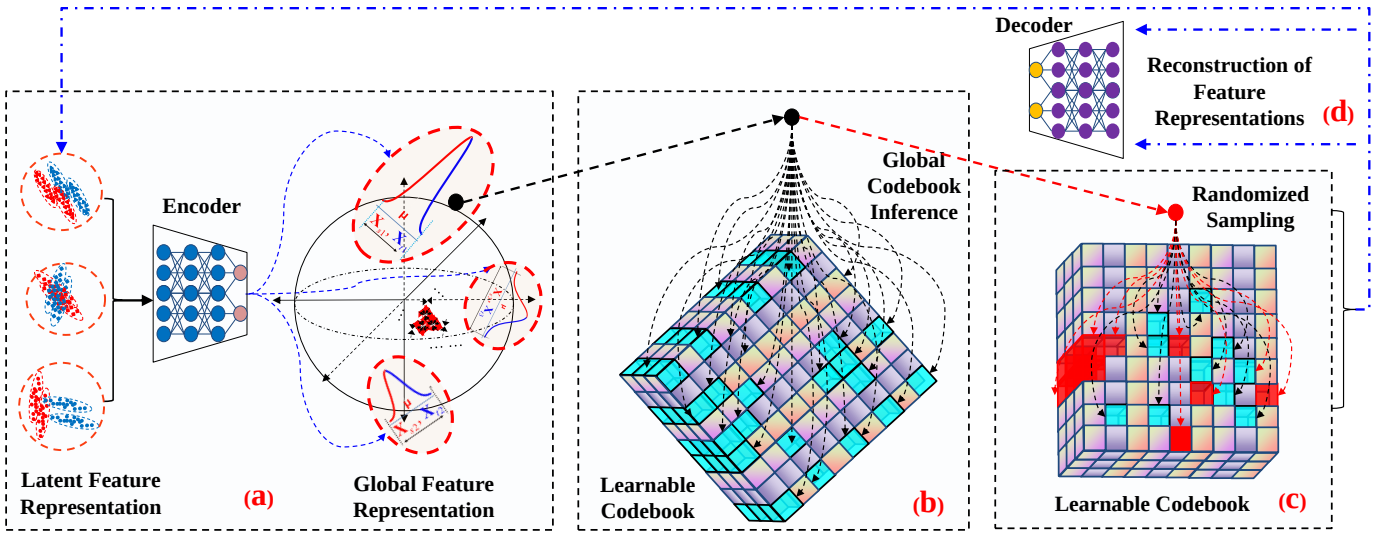

Fig. 3: Fig.3(a) illustrates that class-wise distribution constraints simplify decision boundary optimization but increase the risk of posterior collapse. To mitigate this, Fig.3(b) adopts *Global Codebook Learning*, where entropy-regularized, diverse dictionary associations prevent codeword collapse. Fig.3(c) further introduces *Randomized Sampling*, with red-highlighted blocks denoting stochastic activations that enhance latent diversity. Finally, Fig.3(d) refines the latent representations through reconstruction, promoting more robust and expressive feature embeddings.

in Fig. 3(c), where randomly activated codewords are marked in red, this mechanism promotes diverse codeword utilization and preserves latent expressiveness by preventing uniform assignments to shared dictionary elements. Consequently, it robustly mitigates *posterior collapse* even under strong variance constraints.

Feature Reconstruction Regularized Feature Embedding:

To further ensure that codebook-refined features retain sufficient semantic information, we additionally impose a reconstruction constraint to accurately reconstruct their corresponding inputs as illustrated in Fig. 3(d).

This reconstruction regularization serves two purposes: **P.1** facilitating the search for optimal embeddings within the variance-constrained distributions defined in Eq. (9) for smooth adaptation; and **P.2** encouraging the learned latent distributions to capture rich and consistent cross-domain semantics. The resulting generative capacity further supports the sample augmentation strategy introduced in Section III-B4, which plays a critical role in mitigating pseudo-label noise for robust DA.

4) Generative Augmentation with Entropy-Filtered Pseudo Labels for Robust Domain Adaptation: In the unsupervised domain adaptation (UDA) setting, pseudo-labels for the target domain are generated by a classifier trained on the source domain. This inevitably introduces label noise, which may compromise both the conditional distribution alignment in Section III-B2 and subsequent labeling function optimization. A straightforward remedy is to discard highly confused target samples based on entropy-based confidence scores, computed as $H(\hat{y}_\mathcal{T}) = -\sum_{c=1}^{C} P(\hat{y}_\mathcal{T} = c \mid \mathcal{G}(x_\mathcal{T})) \log P(\hat{y}_\mathcal{T} = c \mid \mathcal{G}(x_\mathcal{T}))$. While this filtering mitigates the impact of noisy pseudo-labels, it may also result in insufficient target-domain coverage, weakening the model's ability to optimize robust decision boundaries. To address this, we augment the training data by generating additional target samples from the high-confidence instance set $\mathcal{G}(x_\mathcal{T})$ with pseudo-labels $\hat{y}_\mathcal{T}$. These augmented samples are designed to satisfy two objectives: ***Objective.1***: faithfully represent the target domain distribution; ***Objective.2***: ensure sufficient sample diversity. For ***Objective.1***, we apply Gaussian perturbation to create augmented features $\mathcal{G}(x_\mathcal{T})' = \mathcal{G}(x_\mathcal{T}) + \epsilon$ where $\epsilon \sim \mathcal{N}(0, \sigma^2\mathbf{I})$, and enforce distributional consistency by aligning the perturbed and original features: $\mathcal{P}(\mathbf{E}(\mathcal{G}(x_\mathcal{T})') \mid \hat{y}_\mathcal{T} = c) \approx \mathcal{P}(\mathbf{E}(\mathcal{G}(x_\mathcal{T})) \mid \hat{y}_\mathcal{T} = c)$ under the shared variance-constrained prior $\mathcal{P}_{\text{epoch}}(\mathcal{G}(x))_{x \in \mathcal{D}_\mathcal{S}^{(i)}} \sim \mathcal{N}(\boldsymbol{\mu}_i, \frac{1}{C}\mathbf{I})$. For ***Objective.2***, the augmented samples are further reconstructed through the global codebook learning and randomized sampling mechanisms introduced in Section III-B3, whose stochastic sampling enhances diversity among the generated samples and better represents the true feature distribution.

In summary, this strategy jointly filters highly confused target samples via entropy scoring to avoid potential negative transfer, while augmenting reliable, class-consistent, and diversified target samples to support robust cross-domain decision boundary optimization.

5) Adversarial Optimization for Joint Feature-Label Distribution Alignment: Although both Section III-B2 and Section III-B3 implicitly align the conditional distributions $\{\mathcal{P}_\mathcal{S}(\mathcal{X} \mid \mathcal{Y}), \mathcal{P}_\mathcal{T}(\mathcal{X} \mid \mathcal{Y})\}$ via global class-wise variance constraints, they lack explicit label-guided modeling for discriminative cross-domain decision optimization. To address this, we introduce a conditional adversarial optimization strategy inspired by **CDAN** [44], which explicitly aligns the joint distributions $\mathcal{P}_\mathcal{S}(\mathcal{X}, \mathcal{Y})$ and $\mathcal{P}_\mathcal{T}(\mathcal{X}, \mathcal{Y})$ to simultaneously capture both sample and label structure for robust decision-boundary optimization. Specifically, CDAN fuses the feature

vector $\mathbf{f}$ and label embedding $\Phi(y)$ using a multilinear conditioning operator: $\mathbf{h} = \mathcal{K}(\mathbf{f}, \Phi(y))$, where $\mathcal{K}(\cdot)$ denotes a learnable kernel mapping. This formulation enables effective adversarial training that jointly captures semantic alignment and discriminative structure, thereby promoting more reliable cross-domain decision making.

C. Overall Optimization

The overall optimization strategy of **GVI-DA** is synthesized in Fig. 4 where blue arrows illustrate the data flow during optimization, while red arrows highlight the five primary loss functions involved in the training process. The **data flow** proceeds as follows: Given the cross-domain datasets $\mathcal{X}_\mathcal{S}$ and $\mathcal{X}_\mathcal{T}$, samples are first mapped by the feature extractor $\mathcal{G}(\cdot)$ to latent representations $\mathcal{G}(x_\mathcal{S})$ and $\mathcal{G}(x_\mathcal{T})$. These features are then processed by the encoder $\mathbf{E}(\cdot)$ to produce a batch-level embedding distribution $\mathcal{P}_{batch}\big(\mathbf{E}(\mathcal{G}(x))\big)_{x\in\mathcal{D}_\mathcal{S}^{(i)}\cup\mathcal{D}_\mathcal{T}^{(i)}}$, where a variational inference constraint is applied to facilitate global conditional distribution alignment. To mitigate posterior collapse, we further introduce a global codebook learning strategy, which updates the feature space into discrete representations $\tilde{P}(e_k)$ through stochastic quantization and prior alignment.

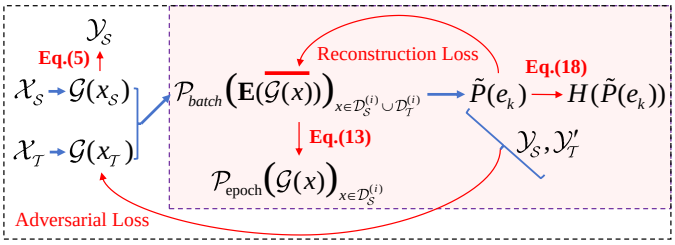

Fig. 4: The overall optimization procedure of **GVI-DA**.

The main optimization objectives of **GVI-DA** include five loss functions. Among them, ***L.1*** - the structural risk minimization loss (as Eq. (2) in Section III-B1) and ***L.2*** - the adversarial loss (introduced in Section III-B5) are commonly adopted in DA literature. Beyond these two losses, **GVI-DA** introduces three additional losses that form the core of our proposed global variational inference framework. These three objectives, highlighted in the *red-shaded area* of Fig. 4, are formally expressed in Eq. (16):

$$\begin{aligned}
&\log p_\varphi(\mathbf{x}) \geq \underbrace{\mathbb{E}_{q_\theta(\mathbf{Z}|\mathbf{x})} H(\hat{P}_\psi(\mathbf{CB}_q|\mathbf{PFD}) q_\theta(\mathbf{PFD} \mid \mathbf{Z}))}_{\textit{codebook entropy loss}} - d_{e_k} \log K \\
&+\mathbb{E}_{q_\theta(\mathbf{Z}|\mathbf{x}) q_\theta(\mathbf{PFD}|\mathbf{Z}) \hat{P}_\psi(\mathbf{CB}_q|\mathbf{PFD})} \left[\begin{array}{l} \underbrace{\log p_\varphi(\mathbf{x}|\mathbf{CB}_q)}_{\textit{reconstruction loss}} + \\ \underbrace{\log \frac{p_\psi(\mathbf{PFD} \mid \mathbf{CB}_q) p_\psi(\mathbf{Z} \mid \mathbf{PFD})}{q_\theta(\mathbf{Z}|\mathbf{x})}}_{\textit{global alignment loss}} \end{array} \right] \\
&s.t. \mathbf{x} = \mathcal{P}_{batch}(\mathcal{G}(x))_{x\in\mathcal{D}_\mathcal{S}^{(i)}\cup\mathcal{D}_\mathcal{T}^{(i)}}, \quad \mathbf{PFD} = \mathcal{P}_{\text{epoch}}(\mathcal{G}(x))_{x\in\mathcal{D}_\mathcal{S}^{(i)}}, \\
&\mathbf{CB}_q = \tilde{P}(e_k \mid \mathbf{E}(\mathcal{G}(x))), \quad \mathbf{Z} = \mathcal{P}_{batch}(\mathbf{E}(\mathcal{G}(x)))_{x\in\mathcal{D}_\mathcal{S}^{(i)}\cup\mathcal{D}_\mathcal{T}^{(i)}}
\end{aligned} \tag{16}$$

where $d_{e_k} \log K$ is a constant term, with d_{e_k} denoting the dimensionality of the codebook entry, and K representing the total number of codebook entries. As illustrated in both Fig. 4 and Eq. (16), ***L.3*** - the *global alignment loss* (Eq. (9)) enforces cross-domain alignment of global conditional distributions, ***L.4*** - the *codebook entropy loss* (Eq. (14)) promotes diverse codebook utilization to alleviate posterior collapse, and ***L.5*** - the *reconstruction loss*, detailed in Section III-B3, refines latent embeddings by encouraging selection of optimal feature locations to minimize training error bounds. Notably, these three objectives naturally emerge from the variational inference perspective, as they can be directly derived from the evidence lower bound (ELBO) under the maximum likelihood estimation constraint. Due to space limitations, the full derivation of Eq. (16) is provided in the supplementary materials, where we further explain the theoretical rationale underlying the design of the three loss terms.

IV. Experiments

This section offers a comprehensive evaluation of the proposed method, including benchmarks and features (Sect.IV-A), experimental setup (Sect.IV-B), baseline comparisons (Sect.IV-C), and performance analysis against state-of-the-art methods (Sect.IV-D). In addition, Sect.IV-E provides in-depth insights into the role of continuous priors, codebook size sensitivity, robustness to target-domain pseudo-label noise, and computational efficiency, further enhancing the understanding of our approach.

A. Dateset Description

Digits: We evaluate **GVI-DA** on three standard digit datasets [44], [37]: *MNIST* (M), *USPS* (U), and *SVHN* (S). *MNIST* provides 60,000 training and 10,000 testing grayscale handwritten digits. *USPS* offers 9,298 samples at lower resolution. *SVHN* contains over 600,000 color digits from natural scenes, exhibiting high noise and background variation. Tasks like $S \to M$ and $M \to U$ reflect domain gaps in style, resolution, and noise. **Office-31**[1]: A widely used DA benchmark with 4,110 images from three domains: *Amazon* (A), *Webcam* (W), and Dslr (D). It defines six transfer tasks across domains, covering shifts in resolution and acquisition conditions. **ImageCLEF-DA**[2]: This dataset includes 12 object categories shared by three domains: *Caltech-256* (C), *ImageNet ILSVRC 2012* (I), and *Pascal VOC 2012* (P). The six transfer tasks evaluate adaptation under differences in resolution, content, and background complexity. **Office-Home**: A more challenging benchmark [72] comprising four domains, *Art* (Ar), *Clipart* (Cl), *Product* (Pr), and *Real-World* (Rw), each with 65 categories. It defines 12 transfer tasks that capture substantial domain discrepancies in style and modality.

B. Experimental Setup

For experiments on the **Digits** datasets, we employed a variant of the LeNet architecture [25] as the feature extractor. For all image recognition tasks, the backbone encoder was a ResNet-50 [23] pretrained on ImageNet, with the final fully connected layer replaced by a domain-specific classifier. The domain discriminator followed a *FC-ReLU-DROP-FC-ReLU-DROP-FC-Sigmoid* structure, and the task classifier was implemented as a standard softmax layer. Optimization for digit recognition tasks was performed using mini-batch

[1] https://faculty.cc.gatech.edu/~judy/domainadapt/
[2] http://imageclef.org/2014/adaptation

stochastic gradient descent (SGD) with a momentum of 0.9, a weight decay of 5×10^{-4}, and a batch size of 64. The learning rate schedule followed the setting used in [53]. For the **Office-31** dataset (31 classes), learning rates were adapted based on domain pair difficulty. Specifically, for pairs where the source was *webcam* and the target was either *dslr* or *amazon*, or vice versa, the learning rate was set to 0.001. For more divergent pairs such as *amazon* $\rightarrow$ *dslr* or *dslr* $\rightarrow$ *webcam*, the learning rate was reduced to 0.0003. For the **ImageCLEF-DA** dataset (12 shared categories across *ImageNet*, *Caltech-256*, and *Pascal VOC*), the learning rate was consistently set to 0.001. For the **Office-Home** dataset (65 categories across *Art*, *Clipart*, *Product*, and *Real-World*), the learning rate was also fixed at 0.001 across all adaptation tasks. Across all datasets, GVI-DA employed a shared feature encoder $\mathcal{G}(\cdot)$, an embedding network $\mathbf{E}(\cdot)$, and a discrete codebook with $K = 256$ entries of dimension $d_{e_k} = 256$ for cross-domain image classification. The entire network was optimized using SGD with momentum 0.9, weight decay 5×10^{-4}, and batch size 64. Following standard practice [44], [54], [50], [51], classification accuracy on the target domain was used as the evaluation metric, computed as:

$$\text{Accuracy} = \frac{|\{x \in \mathcal{D}_T \mid \hat{y}(x) = y(x)\}|}{|\mathcal{D}_T|}, \tag{17}$$

where $\mathcal{D}_T$ denotes the target test domain, $\hat{y}(x)$ is the predicted label, and $y(x)$ is the ground-truth label for each test sample x.

With the growing adoption of Vision Transformers (**ViTs**) [14] in visual recognition tasks due to their strong global modeling capabilities, we integrate our proposed global variational inference framework into transformer-based backbones to further improve domain adaptation performance. Specifically, we adopt the Transferable Vision Transformer (**TVT**) [81] as the base architecture and embed our inference module into its intermediate representations, resulting in the **TVT-GVI** variant. This design evaluates whether our generative alignment mechanism can complement the token-level semantics and global receptive fields inherent in ViT models. For a fair comparison with existing UDA methods, we use the ViT-B/16 backbone pre-trained on ImageNet-21K, with input images resized to 256×256. Experiments are conducted on the Office-31 and Office-Home datasets using standard source-target splits. For Office-31, we set the number of classes to 31, batch size to 16, and train for 10,000 steps with 1,000 warm-up steps using a learning rate of 0.05. For Office-Home, we follow a similar setup with 65 classes and a slightly higher learning rate of 0.06 to account for increased domain diversity.

C. Baseline Methods

The proposed **GVI-DA** method is compared with **thirty-eight** popular methods from recent literatures: (1) **GAN-DA-2025** [53]; (2) **PDBS-2024** [38]; (3) **DOLL-DA-2024** [52]; (4) **TLSR-2024** [49]; (5) **DSACDIC-2024** [90]; (6) **TVT-2023** [81]; (7) **P2TCP-2023** [16]; (8) **BPTN-2023** [75]; (9) **PGFL-2023** [15]; (10) **DRDA-2023** [28]; (11) **SUDA-2022** [85]; (12) **CaCo-2022** [27]; (13) **CDTrans-2021** [79]; (14) **ViT-2020** [14]; (15) **DSAN-2020** [92]; (16) **ATM-2020** [37]; (17) **GSDA-2020** [26]; (18) **CAT-2019** [13]; (19) **TPN-2019** [57]; (20) **BSP-2019** [8]. (21) **SWD-2019** [36]; (22) **TADA-2019** [76]; (23) **BSP-2019** [76]; (24) **MADA-2018** [58]; (25) **CDAN-2018** [44]. (26) **MCD-2018** [61]; (27) **GTA-2018** [62]; (28) **CyCADA-2018** [25]; (29) **MSTN-2018** [78]; (30) **UNIT-2017** [41]; (31) **ADDA-2017** [68]; (32) **RTN-2016** [47]; (33) **JAN-2016** [46]; (34) **D-CORAL-2016** [64]; (35) **DRCN-2016** [20]; (36) **CoGAN-2016** [42]; (37) **DANN-2016** [18]; (38) **DAN-2015** [43].

Whenever possible, the reported performance scores of the **Thirty-eight** methods from the literature are directly collected from their original papers or previous research [44], [8], [53], [81]. These scores are assumed to represent their *best* performance.

D. Experimental Results and Discussion

*1) **Experiments on the Digits DataSet**:* MNIST, USPS, and SVHN are three widely used digit classification benchmarks that pose significant DA challenges. While MNIST and USPS consist of grayscale handwritten digits with different resolutions and styles, SVHN comprises color images of street view house numbers with complex backgrounds and noise. Table II summarizes the DA results across these datasets, with the best-performing scores highlighted in red. From the results, we make the following observations:

- **DSAN** addresses batch sampling inconsistency by introducing soft labels over the full class probability space as importance weights, enabling weighted conditional alignment. This enhances global sample awareness and achieves a competitive accuracy of 94.1%. Building on this, **CDAN** incorporates adversarial training to replace manual kernel design and employs multilinear conditioning to model the joint distribution of features and labels, further improving accuracy to 94.3%. **ATM** advances **CDAN** by integrating adversarial learning with statistical alignment. It introduces the *Maximum Density Divergence (MDD)* loss, theoretically defined as $\mathcal{L}_{\text{MDD}} = \sup_{f \in \mathcal{F}} (\mathbb{E}_{x \sim \mathcal{D}_S}[f(x)] - \mathbb{E}_{x \sim \mathcal{D}_T}[f(x)])$, which promotes both intra-class compactness and domain-invariant representations. As a result, ATM achieves a state-of-the-art accuracy of 99.0% on the $U \rightarrow M$ task and an average of 97.1% across all settings.
- To enhance global knowledge awareness for robust domain adaptation, **DOLL-DA** constructs class-conditional global priors based on label distributions. However, its shallow modeling paradigm limits the discriminative capacity of learned features. **GAN-DA** addresses this by introducing the global anchor term **PFR**, which encodes cross-domain conditional distributions and improves the average accuracy to 97.2%. **GVI-DA** further advances this direction by replacing discrete anchors with variational, data-dependent class priors that better reflect intrinsic data structures and explicitly minimize the training error bound. In addition, it filters low-confidence pseudo-labeled target samples and regenerates reliable ones to suppress negative transfer, resulting in an improved accuracy of 97.3%.

TABLE II: Accuracy (%) on Digital Image Datasets

Method	M→U	U→M	S→M	Average
DAN	80.3	77.8	73.5	77.2
DRCN	91.8	73.7	82.0	82.5
CoGAN	91.2	89.1	–	–
ADDA	89.4	91.0	76.0	85.2
MCD	94.2	94.1	96.2	94.8
CAT	90.6	90.6	98.1	93.1
TPN	92.1	94.1	93.0	93.1
BSP	93.3	95.3	91.4	93.3
GTA	92.8	90.8	92.4	92.0
CyCADA	95.6	96.5	96.4	96.2
UNIT	96.0	93.0	90.3	93.2
MSTN	92.9	–	91.7	–
CDAN	95.6	98.0	89.2	94.3
DSAN	96.9	95.3	90.1	94.1
ATM	96.1	**99.0**	96.9	97.1
DOLL-DA	97.2	86.9	87.8	90.6
GAN-DA	96.2	98.6	96.7	97.2
GVI-DA	**97.4**	98.5	**98.2**	**98.0**

*2) **Experiments on the ImageCLEF-DA Dataset:*** ImageCLEF-DA comprises three domains, Caltech-256 (C), ImageNet ILSVRC 2012 (I), and Pascal VOC 2012 (P), each containing 600 images across 12 shared categories. Following the standard evaluation protocol [53], [37], we report the results in Table III. **DSAN** mitigates batch-wise inconsistency by leveraging full probability-space modeling for conditional alignment, achieving an accuracy of 90.2%. **CDAN** adopts an adversarial learning strategy to align conditional distributions via multilinear conditioning, resulting in 87.7% accuracy. **GAN-DA** further improves **CDAN** by incorporating global anchors to enforce global cross-domain consistency, reaching 90.0%. However, **GAN-DA**'s reliance on discrete priors may yield non-smooth approximations of class-conditional distributions, and its sensitivity to highly ambiguous pseudo-labeled target samples can induce negative transfer.

To address these issues, the proposed **GVI-DA** replaces discrete anchors with variationally learned, continuous priors and selectively filters low-confidence target samples by regenerating reliable pseudo-labeled instances. This leads to improved robustness while achieving 90.55% accuracy.

TABLE III: Accuracy (%) on ImageCLEF-DA Dataset

Method	I→P	P→I	I→C	C→I	C→P	P→C	Average
ResNet	74.8	83.9	91.5	78.0	65.5	91.2	80.8
DAN	75.0	86.2	93.3	84.1	69.8	91.3	83.3
DANN	75.0	86.0	96.2	87.0	74.3	91.5	85.0
D-CORAL	76.9	88.5	93.6	86.8	74.0	91.6	85.2
JAN	76.8	88.0	94.7	89.5	74.2	92.2	85.9
MADA	75.0	87.9	96.0	88.8	75.2	92.2	85.9
CDAN	77.7	90.7	97.7	91.3	74.2	94.3	87.7
TLSR	76.1	89.2	94.9	90.7	74.9	92.6	86.4
CAT	76.7	89.0	94.5	89.8	74.0	93.7	86.3
BPTN	78.6	92.1	96.6	91.3	77.8	96.1	88.8
DSAN	80.2	**93.3**	97.2	93.8	**80.8**	95.9	90.2
ATM	80.3	92.9	98.6	93.5	77.8	96.7	90.0
GAN-DA	**81.2**	91.5	98.7	92.4	76.9	95.9	89.4
GVI-DA	80.9	91.7	**99.5**	**94.2**	79.3	**97.7**	**90.55**

*3) **Experiments on the Office-31 Dataset:*** **Office-31** is a widely used benchmark for UDA, consisting of 31 office-related categories across three domains: Amazon, Webcam, and Dslr. Table IV summarizes the accuracy of representative UDA methods. The upper section of the table includes methods based on the **ResNet-50** backbone. The source-only **ResNet-50** baseline achieves 76.1% accuracy, highlighting the need for adaptation. **CDAN** leverages adversarial training with multilinear conditioning to align joint distributions, reaching 87.7%. **DSAN** models the full class-probability space to reduce batch-level inconsistency, improving to 88.4%. **ATM** further introduces intra-class compactness and domain-invariance via Maximum Density Divergence (MDD), achieving 89.8%. **GAN-DA** and **DRDA** explore global conditional alignment strategies: the former uses predefined anchors, and the latter employs radial distribution regularization, both achieving 90.2%. Our proposed **GVI-DA** replaces rigid anchors with variationally inferred global priors and augments high-confidence target samples, leading to 91.0% accuracy with improved alignment and robustness.

The lower section of Table IV presents the UDA results using the **ViT** backbone. The baseline **ViT** model achieves an accuracy of 91.1%, benefiting from global context modeling through self-attention and large-scale pretraining on ImageNet-21K. **CDTrans** introduces adversarial objectives at both the feature and prediction levels, improving performance by 1.5%. **TVT** further enhances alignment through patch-wise adversarial training over 16×16 visual tokens and achieves an additional gain of 2.8%. To evaluate the generalizability of global alignment strategies, we extend the anchor-based **GAN-DA** approach to the TVT backbone, resulting in **GAN-TVT**. This variant applies global anchor regularization to the latent representations. However, the performance improvement is limited. We attribute this to two main factors. First, ViT backbones already encode global semantic priors through self-attention and extensive pretraining, which reduces the additional benefit of external alignment. Second, the fixed discrete anchors in **GAN-DA** fail to adapt to the intrinsic geometry of cross-domain feature distributions, which imposes a stronger optimization burden.

In contrast, our proposed **GVI-TVT** employs a variational inference framework to construct a continuous class-conditional prior $p(\hat{\phi}_c \mid \boldsymbol{\theta})$ that better reflects the semantic structure of the target domain. This enables smoother and more expressive alignment. **GAN-TVT** minimizes the training error bound through a hybrid objective that combines reconstruction likelihood with a regularized variational posterior. It also samples discrete codebook entries to generate high-confidence target-domain features, thereby improving robustness under pseudo-label noise. This design complements the token-level modeling of ViTs while injecting global structure into the alignment process. As a result, **GVI-TVT** achieves an accuracy of 95.4%, establishing a new state of the art under transformer-based UDA settings.

*4) **Experiments on the Office-Home Dataset:*** **Office-Home**, introduced by DAH [72], is a challenging benchmark comprising four distinct domains and 65 object categories, resulting in 12 cross-domain adaptation tasks. Table V summarizes the performance comparison of our proposed methods against several state-of-the-art approaches. The upper portion of the table presents methods based on the ResNet-50 backbone. Among them, **GSDA** achieves a strong accuracy of 70.3% by mitigating both marginal and conditional domain gaps through hierarchical group-wise alignment. Our proposed **GAN-DA** further improves performance to 70.6%, benefiting from a predefined global anchor strategy that regularizes

TABLE IV: Accuracy (%) on Office-31 Dataset

Method	A→W	D→W	W→D	A→D	D→A	W→A	Average
ResNet-50	68.4	96.7	99.3	68.9	62.5	60.7	76.1
DAN	80.5	97.1	99.6	78.6	63.6	62.8	80.4
RTN	84.5	96.8	99.4	77.5	66.2	64.8	81.6
DANN	82.0	96.9	99.1	79.7	68.2	67.4	82.2
ADDA	86.2	96.2	98.4	77.8	69.5	68.9	82.9
JAN	85.4	97.4	99.8	84.7	68.6	70.0	84.3
GTA	89.5	97.9	99.8	87.7	72.8	71.4	86.5
P2TCP	90.1	99.1	99.2	90.0	75.5	74.8	88.1
BPTN	96.7	98.4	**100.0**	91.7	73.1	75.0	89.2
DSACDIC	95.1	98.6	**100.0**	91.8	76.2	75.5	89.5
PDBS	93.6	98.6	99.9	93.3	71.2	72.1	88.1
CDAN	94.1	98.6	**100.0**	92.9	71.0	69.3	87.7
D-CORAL	77.7	97.6	99.7	81.1	64.6	64.0	80.8
SUDA	91.0	98.8	**100.0**	91.9	72.69	72.3	87.8
CaCo	89.7	98.4	**100.0**	91.7	73.1	72.8	87.6
MADA	90.0	97.4	99.6	87.8	70.3	66.4	85.3
PGFL	90.7	99.1	99.8	93.8	78.1	76.4	89.6
ATM	95.7	99.3	**100.0**	96.4	74.1	73.5	89.8
GSDA	95.7	99.1	**100.0**	94.8	73.5	74.9	89.7
SWD	90.4	98.7	**100.0**	94.7	70.3	70.5	87.4
DSAN	93.6	98.3	**100.0**	90.2	73.5	74.8	88.4
DRDA	95.8	98.8	**100.0**	94.5	75.6	**76.6**	90.2
GAN-DA	95.4	**99.6**	**100.0**	95.4	75.9	74.6	90.2
GVI-DA	**96.2**	**99.6**	**100.0**	**97.9**	**76.1**	75.9	**91.0**
ViT	91.2	99.2	**100.0**	93.6	80.7	80.7	91.1
TVT	96.4	**99.4**	**100.0**	96.4	84.9	86.1	93.9
CDTrans	96.7	99.0	**100.0**	97.0	81.1	81.9	92.6
GAN-TVT	96.1	99.0	**100.0**	96.7	85.9	85.9	93.9
GVI-TVT	**98.7**	99.1	**100.0**	**98.7**	**89.2**	**86.9**	**95.4**

the conditional feature space and supports decision-boundary refinement. Building on this, **GVI-DA** introduces a global variational inference framework to learn a continuous class-conditional prior, $p(\hat{\phi}_c \mid \boldsymbol{\theta})$, which more effectively models the intrinsic cross-domain structure. By minimizing the training error bound via reconstruction likelihood and adaptive posterior sampling, **GVI-DA** promotes smoother global alignment and improves target-domain generalization, reaching an accuracy of 70.9%.

The lower section of Table V reports DA performance using the ViT-based architecture. Benefiting from self-attention and large-scale pretraining, the vanilla **ViT** model achieves a strong average accuracy of 75.5%, surpassing all ResNet-based DA baselines even without any domain alignment modules. This confirms that ViT can partially capture domain-invariant semantics through global receptive modeling. On top of this, **CDTrans** integrates adversarial alignment at both the feature and label levels, effectively mitigating cross-domain distribution shifts and achieving 80.5% accuracy. **TVT** further improves the result to 83.6% by enforcing patch-level adversarial learning over tokenized image regions, enabling fine-grained alignment across domains. To enhance global conditional distribution awareness under TVT, **GAN-TVT** incorporates handcrafted discrete anchors into the latent space and reaches 83.9%. However, the improvement is marginal ($\Delta = 0.3\%$), as ViT backbones inherently encode global priors, and the handcrafted anchors in **GAN-DA** fail to adapt to the intrinsic geometry of cross-domain features, increasing the regularization burden.

In contrast, the proposed **GVI-TVT** framework introduces a variational inference mechanism to learn a continuous class-conditional prior $p(\hat{\phi}_c \mid \boldsymbol{\theta})$ that aligns with the latent space of ViT. This prior facilitates semantically consistent target embedding by minimizing the training error bound via a hybrid objective combining likelihood reconstruction and posterior regularization. Moreover, **GVI-TVT** improves robustness by generating high-confidence target samples from learned codebooks, effectively mitigating pseudo-label noise. As a result, **GVI-TVT** achieves a state-of-the-art accuracy of 86.9%, demonstrating its scalability and effectiveness under transformer-based architectures.

E. Empirical Analysis

While the proposed **GVI-DA** achieves state-of-the-art performance across 38 DA tasks on four benchmarks, several open questions remain to further elucidate its underlying principles: **Q1: Discrete vs. Continuous Priors.** *Can the performance gains of continuous priors be replicated in anchor-based models, or is variational inference essential for their effectiveness?* **Q2: Computational Efficiency.** *What is the actual training overhead introduced by variational inference and sample generation, and how does it affect scalability compared to GAN-DA?* **Q3: Codebook Size Sensitivity.** *How does codebook size impact performance, memory, and computation, and what is the optimal trade-off?* **Q4: Target Sample Generation.** *To what extent does target sample generation contribute to robustness, particularly under varying pseudo-label noise levels?* **Q5: Variational Inference vs. Diffusion Modeling.** *Could diffusion-based generative models outperform variational inference in capturing global conditional distributions for DA?* **Q6: Loss Term Contribution.** *How do reconstruction, global alignment, and entropy regularization individually contribute to overall performance?* We explore these questions through targeted ablation studies and empirical analyses to better understand the driving factors behind GVI-DA's effectiveness.

Q1: Discrete vs. Continuous Priors: To better examine **Q1**, we propose a variant termed *Noise Perturbation Enhanced Anchor-based Domain Adaptation* (**NPA-DA**), which aims to test whether replacing discrete anchor points with continuous priors, without using variational inference, can yield comparable improvements in anchor-based DA frameworks. Anchor-based DA relies on globally stable class-conditional priors to mitigate inconsistencies caused by mini-batch sampling. Following the design of **GAN-DA**, we construct predefined anchors f^c_{NPA} in the feature space based on cross-domain feature dimensionality. As illustrated in Fig.5(a), for a task such as **SVHN→MNIST**, we generate C anchors using block-wise binary vectors:

$$f^c_{\text{NPA}} = [\underbrace{0,\ldots,0}_{51},\ldots,\underbrace{1,\ldots,1}_{\text{slot } c},\ldots,\underbrace{0,\ldots,0}_{51}] \in \mathbb{R}^{C\times 51}, \quad (18)$$

where each anchor activates a distinct slot corresponding to class c, forming an orthogonal prior structure. This design serves as a continuous prior surrogate and enables us to isolate the role of variational inference from that of prior continuity. As shown in Table VI, **NPA+X** denotes a CDAN-based variant augmented with the anchors f^c_{NPA}, where X specifies the standard deviation of Gaussian noise $\mathcal{N}(0, X^2)$ injected to perturb the anchor distribution. In particular, **NPA+1** applies MMD-based alignment to match cross-domain features to the continuous prior distribution $\delta(f^c_{\text{NPA}}) \otimes \mathcal{N}(0,1)$. Based on the results in Table VI, we draw the following conclusions:

TABLE V: Accuracy (%) on Office-Home Dataset

Method	Ar→Cl	Ar→Pr	Ar→Rw	Cl→Ar	Cl→Pr	Cl→Rw	Pr→Ar	Pr→Cl	Pr→Rw	Rw→Ar	Rw→Cl	Rw→Pr	Average
ResNet	34.9	50.0	58.0	37.4	41.9	46.2	38.5	31.2	60.4	53.9	41.2	59.9	46.1
DAN	43.6	57.0	67.9	45.8	56.5	60.4	44.0	43.6	67.7	63.1	51.5	74.3	56.3
MCD	46.9	64.1	77.6	56.1	62.4	65.5	58.9	45.8	80.0	73.3	49.8	83.1	63.6
CDAN	50.7	70.6	76.0	57.6	70.0	70.0	57.4	50.9	77.3	70.9	56.7	81.6	65.8
TADA	53.1	72.3	77.2	59.1	71.2	72.1	59.7	53.1	78.4	72.4	60.0	82.9	67.6
GSDA	61.3	**76.1**	**79.4**	**65.4**	73.3	**74.3**	**65.0**	53.2	80.0	72.2	60.6	83.1	70.3
DANN	45.6	59.3	70.1	47.0	58.5	60.9	46.1	43.7	68.5	63.2	51.8	76.8	57.6
JAN	45.9	61.2	68.9	50.4	59.7	61.0	45.8	43.4	70.3	63.9	52.4	76.8	58.3
BSP	51.4	68.3	75.9	56.0	67.8	68.8	56.0	49.6	75.8	70.4	57.1	80.6	64.9
DSAN	54.4	70.8	75.4	60.4	67.8	68.0	62.6	**55.9**	78.5	73.8	60.6	83.1	67.6
ATM	52.4	72.6	78.0	61.1	72.0	72.6	59.5	52.0	79.1	73.3	58.9	**83.4**	67.9
GAN-DA	**68.0**	75.9	73.2	63.7	72.5	73.4	61.9	54.0	**83.1**	**73.9**	**64.3**	83.0	70.6
GVI-DA	66.7	71.5	79.2	64.7	**75.5**	72.4	63.9	55.0	**83.1**	73.6	62.3	82.9	**70.9**
ViT	54.7	83.0	87.2	77.3	83.4	85.6	74.4	50.9	87.2	79.6	54.8	88.8	75.5
TVT	74.9	86.8	89.5	82.8	88.0	88.3	79.8	71.9	**90.1**	85.5	74.6	90.6	83.6
CDTrans	68.8	85.0	86.9	81.5	87.1	87.3	79.6	63.3	88.2	82.0	66.0	90.6	80.5
GAN-TVT	71.2	89.0	87.9	86.8	89.2	87.4	79.7	69.5	89.4	87.9	**76.8**	**91.9**	83.9
GVI-TVT	**80.1**	**90.6**	**92.9**	**89.7**	**92.9**	**93.1**	**84.2**	**78.4**	84.9	**90.0**	76.1	90.4	**86.9**

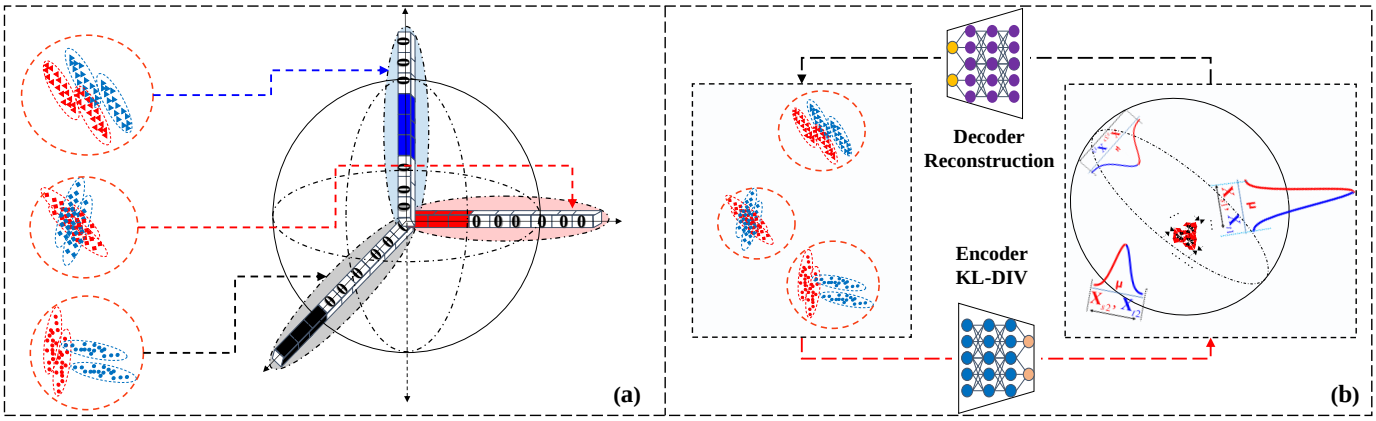

Fig. 5: Fig. 5(a) presents the proposed Noise Perturbation Enhanced Anchor-based DA (**NPA-DA**), while Fig. 5(b) illustrates the variational inference-based variant (**VI-DA**). Both settings are designed to provide deeper insight into the effectiveness of continuous global conditional priors over discrete ones in aligning cross-domain distributions for globally aware adaptation.

TABLE VI: Accuracy (%) for different experimental settings of **NPA-DA** on the **SVHN→MNIST** task.

Method	CDAN	NPA+0	NPA+0.01	NPA+0.1	NPA+0.5	NPA+1	NPA+2
S→M	89.30	94.60	94.60	92.70	93.50	92.10	92.10

NPA+0 outperforms the **CDAN** baseline by 5.3%, validating the role of discrete global anchors in providing stable priors and mitigating batch sampling inconsistency. However, as the noise level increases from 0.01 to 2, performance steadily declines. This suggests two key insights: (1) *perturbing anchors into continuous distributions alone does not ensure smooth alignment*; and (2) increasing prior variance reduces inter-class separability, weakening feature discriminability.

To understand why simply converting discrete priors into continuous distributions is insufficient, and to further explore the effectiveness of continuous priors in GVI-DA, we propose a new DA variant, variational inference enhanced domain adaptation (VI-DA), as illustrated in Fig.5(b). Building upon **NPA-DA**, **VI-DA** incorporates variational inference to enable global alignment of class-conditional distributions across domains. In the 10-class digital image setting, we define ten class-specific continuous priors to guide the alignment of cross-domain sub-distributions. Following the mean-field assumption in VAE, each prior is formulated as: $\mathcal{N}_c(\mathcal{Z}, \mu_c, 0.01\mathbf{I}), \quad \mu_c \in \{1.5, 1.2, 0.9, 0.6, 0.3, 0, -0.3, -0.6, -0.9, -1.2\}$. Each class-specific prior is centered at a distinct mean μ_c, enhancing semantic separability and reducing inter-class overlap. **VI-DA** jointly optimizes two objectives: (1) *KL divergence minimization*, aligning the inferred latent distributions with the predefined priors; (2) *feature reconstruction*, ensuring the latent space retains sufficient semantic information. Specifically, we assume the latent representation of class c from source and target domains, (D_S^c, D_T^c), follows a Gaussian posterior $q(\mathbf{z}) = \mathcal{N}(\mathbf{z}; \tilde{\boldsymbol{\mu}}, \tilde{\boldsymbol{\sigma}}^2\mathbf{I})$, while the corresponding predefined prior is $p(\mathbf{z}) = \mathcal{N}(\mathbf{z}; \boldsymbol{\mu}, \boldsymbol{\sigma}^2\mathbf{I})$. The KL divergence loss for class c is then expressed as:

$$L_{KL}^{(c)} = \int q(\mathbf{z}) \log \frac{q(\mathbf{z})}{p(\mathbf{z})} d\mathbf{z} = \sum_{j=1}^{J} -\frac{1}{2}\log(2\pi\sigma_j^2) - \frac{\tilde{\sigma}_j^2}{2\sigma_j^2} - \frac{(\tilde{\mu}_j - \mu_j)^2}{2\sigma_j^2}, \quad (19)$$

where $\tilde{\mu}_j, \tilde{\sigma}_j$ and μ_j, σ_j denote the j-th elements of the posterior and prior distributions, respectively, and J is the latent dimensionality. Summing over all classes yields the total KL loss: $L_{\text{KL}} = \sum_{c=1}^{10} L_{KL}^{(c)}$. For semantic preservation, we also define a reconstruction loss using the squared difference: $L_{\text{recon}} = \sum_{i=1}^{n} \|x_i - \hat{x}_i\|^2$. To balance accuracy and efficiency, we adopt a lightweight encoder architecture *FC(512-*

256)-ReLU-FC(256-128) and decoder with *FC(64-256)-ReLU-FC(256-512)* for distribution inference. As shown in Table VII, **VI-DA** represents the baseline with each class-conditional prior defined as a Gaussian distribution with covariance $0.01\mathbf{I}$. **VI-DA-(0.0001)** and **VI-DA-(1)** denote variants with smaller and larger covariances, set to $0.0001\mathbf{I}$ and $1\mathbf{I}$, respectively. Based on these results, we draw the following conclusions:

TABLE VII: Accuracy (%) on Digital Image Datasets.

Task	CDAN	NPA+0	VI-DA	VI-DA-(0.0001)	VI-DA-(1)	GVI-DA
M→U	95.6±0.56	96.0±0.82	95.9±0.09	95.4±0.24	96.6±0.12	97.4±0.09
U→M	98.0±0.39	98.2±0.93	99.1±0.07	98.6±0.19	95.6±0.11	98.5±0.05
S→M	89.2±0.64	94.6±0.97	96.0±0.11	95.2±0.13	90.6±0.14	98.2±0.09
Average	94.3	96.2	97.0	96.4	94.2	98.1

In Table VII, all methods are evaluated over five runs, and standard deviations are reported. *compared to **NPA+0**, **VI-DA** consistently achieves higher accuracy with lower variance, underscoring the benefit of continuous conditional priors in cross-domain decision optimization. This advantage arises from the closed-loop variational framework in **VI-DA**, where the predefined priors are co-optimized with the encoder via KL divergence and reconstruction loss. Unlike the fixed, non-adaptive priors in **NPA+X**, which merely provide coarse alignment targets, the priors in **VI-DA** are refined through data-driven inference, resulting in semantically aligned latent spaces and more stable decision boundaries.* Additionally, **VI-DA-(0.0001)** exhibits a 0.6% performance drop compared to **VI-DA**, suggesting that overly constrained prior variance may hinder reconstruction and induce posterior collapse. On the other hand, **VI-DA-(1)** shows a more significant drop of 2.8%, indicating that excessive prior variance weakens class separability and compromises discriminative modeling. Finally, **GVI-DA** outperforms **VI-DA** by 1.1%, benefiting from global codebook learning that alleviates posterior collapse, and from the integration of high-confidence target sample generation that enhances alignment robustness.

Q2: Computational Efficiency: To better reply **Q2**, we conduct a comparative analysis of training efficiency across different DA methods on the ImageCLEF-DA dataset. All experiments are performed under identical hardware conditions using a single NVIDIA RTX 4090 GPU to ensure a fair comparison. For each method, we measure the total training time required to process 2000 batches of cross-domain tasks, as reported in Table VIII. Based on the results, we draw the following observations:

TABLE VIII: Comparison of Training Time Across Different Methods on ImageCLEF-DA Dataset

Methods with 2000 batchs	CDAN	GAN-DA	GVI-DA
Training Time	∼35 minutes	∼42 minutes	∼75 minutes

- **CDAN vs. GAN-DA.** The training times for **CDAN** and **GAN-DA** are relatively similar, recorded at approximately 35 and 42 minutes, respectively. This is because **GAN-DA** introduces only a lightweight global anchor regularization term on top of **CDAN**. The global prior in **GAN-DA** is predefined rather than learned, and it is optimized using a single auxiliary alignment objective. As a result, the increase in computational complexity is minimal.
- **GVI-DA.** In comparison, **GVI-DA** introduces a more principled and expressive modeling framework for global conditional priors based on variational inference. The method involves multiple components: global latent feature encoding via $q_\theta(\mathbf{Z}|\mathbf{x})$, stochastic sampling of codebook entries from $\hat{P}_\psi(\mathbf{CB}_q|\mathbf{PFD})$, and reconstruction of input samples through $p_\varphi(\mathbf{x}|\mathbf{CB}_q)$. These components form a variational training loop driven by the evidence lower bound (ELBO). Although **GVI-DA** requires approximately 75 minutes to train on 2000 batches, almost double the time of **CDAN**, it enables structured optimization over the global conditional latent space, yielding improved training error bounds for decision making.
- **Efficiency-Performance Trade-off.** While **GVI-DA** incurs additional computational cost, this is offset by its significant advantages. Compared to **CDAN**, **GVI-DA** introduces global prior awareness instead of relying solely on local batch-wise alignment. Relative to **GAN-DA**, it replaces heuristic anchor-based priors with learnable variational distributions, offering both theoretical rigor and improved interpretability. As demonstrated throughout the paper, this added complexity leads to superior domain adaptation performance across multiple datasets, justifying the trade-off in computational efficiency.

Due to page limitations, the responses to **Q2** through **Q6** in Sect. IV-E are provided in the supplementary materials under **Appendix.2** to **Appendix.6**, respectively. Additionally, the derivation of the evidence lower bound (ELBO) for the proposed GVI-DA framework is detailed in **Appendix.1**, which presents the step-by-step formulation of Eq. (16) and elucidates the theoretical foundation for the design of the three core loss components.

Due to page limitations, the responses to **Q3** through **Q6** in Sect. IV-E are provided in the supplementary materials under **Appendix.2** to **Appendix.5**, respectively. Additionally, the derivation of the evidence lower bound (ELBO) for the proposed GVI-DA framework is detailed in **Appendix.1**, which presents the step-by-step formulation of Eq. (16) and elucidates the theoretical foundation for the design of the three core loss components.

V. Conclusion

In this paper, we propose **GVI-DA**, a novel framework grounded in the principle of global variational inference, to address the inherent contradiction between batch-wise optimization and the minimization of error bounds in deep learning-based DA models. Compared to previous anchor-based DA strategies, **GVI-DA** enables the learning of a continuous global prior that smoothly unifies cross-domain distributions, rather than coercively aligning them onto discretely predefined anchors. Through feature reconstruction regularization, **GVI-DA** further optimizes latent feature embeddings to tighten the training error bound. Furthermore, **GVI-DA** integrates global codebook learning with randomized sampling to effectively mitigate posterior collapse. By leveraging its generative

capacity, GVI-DA also produces additional high-confidence target-domain samples to alleviate pseudo-labeling errors and enhance adaptation robustness. We systematically derive the theoretical evidence lower bound (ELBO) to validate the proposed optimization mechanisms. Extensive experiments across four benchmarks demonstrate the superior performance of **GVI-DA**, while empirical analyses further elucidate its theoretical and practical advantages.

While this study focuses on validating **GVI-DA** under UDA settings, its core idea of global conditional distribution inference through variational optimization offers broader applicability. This framework can be extended to more general settings such as domain generalization and continual learning, where constructing adaptable global priors across dynamic domains is critical for achieving stable and transferable decision boundaries.

REFERENCES

[1] Jimmy Ba, Murat A Erdogdu, Marzyeh Ghassemi, Shengyang Sun, Taiji Suzuki, Denny Wu, and Tianzong Zhang. Understanding the variance collapse of svgd in high dimensions. In *International Conference on Learning Representations*, 2021. 2, 5, 7

[2] Shai Ben-David, John Blitzer, Koby Crammer, Alex Kulesza, Fernando Pereira, and Jennifer Wortman Vaughan. A theory of learning from different domains. *Machine learning*, 79(1):151–175, 2010. 1

[3] Sam Bond-Taylor, Adam Leach, Yang Long, and Chris G Willcocks. Deep generative modelling: A comparative review of vaes, gans, normalizing flows, energy-based and autoregressive models. *IEEE transactions on pattern analysis and machine intelligence*, 2021. 4

[4] Konstantinos Bousmalis, George Trigeorgis, Nathan Silberman, Dilip Krishnan, and Dumitru Erhan. Domain separation networks. In *Advances in Neural Information Processing Systems*, pages 343–351, 2016. 4

[5] Martin Burger, René Pinnau, Claudia Totzeck, and Oliver Tse. Mean-field optimal control and optimality conditions in the space of probability measures. *SIAM Journal on Control and Optimization*, 59(2):977–1006, 2021. 6

[6] Chaoqi Chen, Luyao Tang, Feng Liu, Gangming Zhao, Yue Huang, and Yizhou Yu. Mix and reason: Reasoning over semantic topology with data mixing for domain generalization. *Advances in Neural Information Processing Systems*, 35:33302–33315, 2022. 2, 4

[7] Haotian Chen, Yonghui Xu, Huanhuan Chen, Yong Liu, Haishu Tan, Yuguang Yan, Han Yu, et al. Multicomponent adversarial domain adaptation: A general framework. *IEEE Transactions on Neural Networks and Learning Systems*, 34(10):6824–6838, 2023. 3

[8] Xinyang Chen, Sinan Wang, Mingsheng Long, and Jianmin Wang. Transferability vs. discriminability: Batch spectral penalization for adversarial domain adaptation. In *International conference on machine learning*, pages 1081–1090. PMLR, 2019. 11

[9] Corinna Cortes and Vladimir Vapnik. Support-vector networks. *Machine learning*, 20:273–297, 1995. 7

[10] Shuhao Cui, Shuhui Wang, Junbao Zhuo, Chi Su, Qingming Huang, and Qi Tian. Gradually vanishing bridge for adversarial domain adaptation. In *Proceedings of the IEEE/CVF conference on computer vision and pattern recognition*, pages 12455–12464, 2020. 4

[11] Valentin De Bortoli, James Thornton, Jeremy Heng, and Arnaud Doucet. Diffusion schrödinger bridge with applications to score-based generative modeling. *Advances in Neural Information Processing Systems*, 34:17695–17709, 2021. 4

[12] Kamil Deja, Tomasz Trzciński, and Jakub M Tomczak. Learning data representations with joint diffusion models. In *Joint European Conference on Machine Learning and Knowledge Discovery in Databases*, pages 543–559. Springer, 2023. 4

[13] Zhijie Deng, Yucen Luo, and Jun Zhu. Cluster alignment with a teacher for unsupervised domain adaptation. In *Proceedings of the IEEE/CVF international conference on computer vision*, pages 9944–9953, 2019. 11

[14] Alexey Dosovitskiy, Lucas Beyer, Alexander Kolesnikov, Dirk Weissenborn, Xiaohua Zhai, Thomas Unterthiner, Mostafa Dehghani, Matthias Minderer, Georg Heigold, Sylvain Gelly, et al. An image is worth 16x16 words: Transformers for image recognition at scale. *arXiv preprint arXiv:2010.11929*, 2020. 11

[15] Yongjie Du, Deyun Zhou, Yu Xie, Yu Lei, and Jiao Shi. Prototype-guided feature learning for unsupervised domain adaptation. *Pattern Recognition*, 135:109154, 2023. 11

[16] Yongjie Du, Ying Zhou, Yu Xie, Deyun Zhou, Jiao Shi, and Yu Lei. Unsupervised domain adaptation via progressive positioning of target-class prototypes. *Knowledge-Based Systems*, 273:110586, 2023. 11

[17] Zhekai Du and Jingjing Li. Diffusion-based probabilistic uncertainty estimation for active domain adaptation. *Advances in Neural Information Processing Systems*, 36, 2024. 4

[18] Yaroslav Ganin, Evgeniya Ustinova, Hana Ajakan, Pascal Germain, Hugo Larochelle, François Laviolette, Mario Marchand, and Victor Lempitsky. Domain-adversarial training of neural networks. *The Journal of Machine Learning Research*, 17(1):2096–2030, 2016. 3, 11

[19] Jin Gao, Jialing Zhang, Xihui Liu, Trevor Darrell, Evan Shelhamer, and Dequan Wang. Back to the source: Diffusion-driven adaptation to test-time corruption. In *Proceedings of the IEEE/CVF Conference on Computer Vision and Pattern Recognition*, pages 11786–11796, 2023. 4

[20] Muhammad Ghifary, W Bastiaan Kleijn, Mengjie Zhang, David Balduzzi, and Wen Li. Deep reconstruction-classification networks for unsupervised domain adaptation. In *Computer Vision–ECCV 2016: 14th European Conference, Amsterdam, The Netherlands, October 11–14, 2016, Proceedings, Part IV 14*, pages 597–613. Springer, 2016. 11

[21] Ian Goodfellow, Jean Pouget-Abadie, Mehdi Mirza, Bing Xu, David Warde-Farley, Sherjil Ozair, Aaron Courville, and Yoshua Bengio. Generative adversarial nets. In *Advances in neural information processing systems*, pages 2672–2680, 2014. 3

[22] Jianzhong He, Xu Jia, Shuaijun Chen, and Jianzhuang Liu. Multi-source domain adaptation with collaborative learning for semantic segmentation. In *Proceedings of the IEEE/CVF Conference on Computer Vision and Pattern Recognition*, pages 11008–11017, 2021. 3

[23] Kaiming He, Xiangyu Zhang, Shaoqing Ren, and Jian Sun. Deep residual learning for image recognition. *arXiv preprint arXiv:1512.03385*, 2015. 3, 10

[24] Jonathan Ho, Ajay Jain, and Pieter Abbeel. Denoising diffusion probabilistic models. *Advances in neural information processing systems*, 33:6840–6851, 2020. 4

[25] Judy Hoffman, Eric Tzeng, Taesung Park, Jun-Yan Zhu, Phillip Isola, Kate Saenko, Alexei Efros, and Trevor Darrell. CyCADA: Cycle-consistent adversarial domain adaptation. In Jennifer Dy and Andreas Krause, editors, *Proceedings of the 35th International Conference on Machine Learning*, volume 80 of *Proceedings of Machine Learning Research*, pages 1989–1998, Stockholmsmässan, Stockholm Sweden, 10–15 Jul 2018. PMLR. 4, 10, 11

[26] Lanqing Hu, Meina Kan, Shiguang Shan, and Xilin Chen. Unsupervised domain adaptation with hierarchical gradient synchronization. In *Proceedings of the IEEE/CVF Conference on computer vision and pattern recognition*, pages 4043–4052, 2020. 11

[27] Jiaxing Huang, Dayan Guan, Aoran Xiao, Shijian Lu, and Ling Shao. Category contrast for unsupervised domain adaptation in visual tasks. In *Proceedings of the IEEE/CVF conference on computer vision and pattern recognition*, pages 1203–1214, 2022. 11

[28] Zenan Huang, Jun Wen, Siheng Chen, Linchao Zhu, and Nenggan Zheng. Discriminative radial domain adaptation. *IEEE Transactions on Image Processing*, 32:1419–1431, 2023. 2, 4, 5, 11

[29] Iris AM Huijben, Wouter Kool, Max B Paulus, and Ruud JG Van Sloun. A review of the gumbel-max trick and its extensions for discrete stochasticity in machine learning. *IEEE transactions on pattern analysis and machine intelligence*, 45(2):1353–1371, 2022. 8

[30] Zhuxi Jiang, Yin Zheng, Huachun Tan, Bangsheng Tang, and Hanning Zhou. Variational deep embedding: An unsupervised and generative approach to clustering. In Carles Sierra, editor, *Proceedings of the Twenty-Sixth International Joint Conference on Artificial Intelligence, IJCAI 2017, Melbourne, Australia, August 19-25, 2017*, pages 1965–1972. ijcai.org, 2017. 4

[31] Mengmeng Jing, Jingjing Li, Ke Lu, Lei Zhu, and Heng Tao Shen. Visually source-free domain adaptation via adversarial style matching. *IEEE Transactions on Image Processing*, 2024. 3

[32] Mengmeng Jing, Jidong Zhao, Jingjing Li, Lei Zhu, Yang Yang, and Heng Tao Shen. Adaptive component embedding for domain adaptation. *IEEE Transactions on Cybernetics*, 2020. 2

[33] Yuhan Kang, Jie Wu, Qiang Liu, Jun Yue, and Leyuan Fang. Transdiff: Heterogeneous domain adaptation for remote sensing segmentation with transfer diffusion. *IEEE Journal of Selected Topics in Applied Earth Observations and Remote Sensing*, 2024. 4

[34] Daniel Kifer, Shai Ben-David, and Johannes Gehrke. Detecting change in data streams. In *Proceedings of the Thirtieth international conference*

on Very large data bases-Volume 30, pages 180–191. VLDB Endowment, 2004. 1

[35] Alex Krizhevsky, Ilya Sutskever, and Geoffrey E Hinton. Imagenet classification with deep convolutional neural networks. In *Advances in neural information processing systems*, pages 1097–1105, 2012. 3

[36] Chen-Yu Lee, Tanmay Batra, Mohammad Haris Baig, and Daniel Ulbricht. Sliced wasserstein discrepancy for unsupervised domain adaptation. In *Proceedings of the IEEE/CVF conference on computer vision and pattern recognition*, pages 10285–10295, 2019. 11

[37] Jingjing Li, Erpeng Chen, Zhengming Ding, Lei Zhu, Ke Lu, and Heng Tao Shen. Maximum density divergence for domain adaptation. *IEEE transactions on pattern analysis and machine intelligence*, 43(11):3918–3930, 2020. 10, 11, 12

[38] Liang Li, Tongyu Lu, Yaoqi Sun, Yuhan Gao, Chenggang Yan, Zhenghui Hu, and Qingming Huang. Progressive decision boundary shifting for unsupervised domain adaptation. *IEEE Transactions on Neural Networks and Learning Systems*, 2024. 11

[39] Shuang Li, Chi Harold Liu, Limin Su, Binhui Xie, Zhengming Ding, CL Philip Chen, and Dapeng Wu. Discriminative transfer feature and label consistency for cross-domain image classification. *IEEE Transactions on Neural Networks and Learning Systems*, 2020. 2

[40] Yaron Lipman, Ricky TQ Chen, Heli Ben-Hamu, Maximilian Nickel, and Matt Le. Flow matching for generative modeling. *arXiv preprint arXiv:2210.02747*, 2022. 4

[41] Ming-Yu Liu, Thomas Breuel, and Jan Kautz. Unsupervised image-to-image translation networks. *Advances in neural information processing systems*, 30, 2017. 11

[42] Ming-Yu Liu and Oncel Tuzel. Coupled generative adversarial networks. In *Advances in neural information processing systems*, pages 469–477, 2016. 11

[43] Mingsheng Long, Yue Cao, Jianmin Wang, and Michael I Jordan. Learning transferable features with deep adaptation networks. In *ICML*, pages 97–105, 2015. 3, 11

[44] Mingsheng Long, Zhangjie Cao, Jianmin Wang, and Michael I Jordan. Conditional adversarial domain adaptation. *Advances in neural information processing systems*, 31, 2018. 9, 10, 11

[45] Mingsheng Long, Jianmin Wang, Guiguang Ding, Sinno Jialin Pan, and S Yu Philip. Adaptation regularization: A general framework for transfer learning. *IEEE Transactions on Knowledge and Data Engineering*, 26(5):1076–1089, 2013. 2

[46] Mingsheng Long, Han Zhu, Jianmin Wang, and Michael I Jordan. Deep transfer learning with joint adaptation networks. *arXiv preprint arXiv:1605.06636*, 2016. 11

[47] Mingsheng Long, Han Zhu, Jianmin Wang, and Michael I Jordan. Unsupervised domain adaptation with residual transfer networks. In *Advances in Neural Information Processing Systems*, pages 136–144, 2016. 11

[48] Mingsheng Long, Han Zhu, Jianmin Wang, and Michael I. Jordan. Deep transfer learning with joint adaptation networks. In *Proceedings of the 34th International Conference on Machine Learning, ICML 2017, Sydney, NSW, Australia, 6-11 August 2017*, pages 2208–2217, 2017. 3

[49] Hao Luo, Zhiqiang Tian, Kaibing Zhang, Guofa Wang, and Shaoyi Du. Semi-supervised domain adaptation via joint transductive and inductive subspace learning. *IEEE Transactions on Multimedia*, 2024. 11

[50] Lingkun Luo, Liming Chen, and Shiqiang Hu. Attention regularized laplace graph for domain adaptation. *IEEE Transactions on Image Processing*, 31:7322–7337, 2022. 2, 6, 11

[51] Lingkun Luo, Liming Chen, Shiqiang Hu, Ying Lu, and Xiaofang Wang. Discriminative and geometry-aware unsupervised domain adaptation. *IEEE Transactions on Cybernetics*, 2020. 2, 3, 6, 11

[52] Lingkun Luo, Shiqiang Hu, and Liming Chen. Discriminative noise robust sparse orthogonal label regression-based domain adaptation. *International Journal of Computer Vision*, 132(1):161–184, 2024. 2, 11

[53] Lingkun Luo, Shiqiang Hu, and Liming Chen. Beyond batch learning: Global awareness enhanced domain adaptation. *IEEE Transactions on Pattern Analysis and Machine Intelligence*, 2025. 1, 2, 3, 4, 5, 11, 12

[54] Lingkun Luo, Xiaofang Wang, Shiqiang Hu, and Liming Chen. Robust data geometric structure aligned close yet discriminative domain adaptation. *CoRR*, abs/1705.08620, 2017. 11

[55] Declan McNamara, Jackson Loper, and Jeffrey Regier. Sequential monte carlo for inclusive kl minimization in amortized variational inference. In *International Conference on Artificial Intelligence and Statistics*, pages 4312–4320. PMLR, 2024. 6

[56] Thibault Modeste and Clément Dombry. Characterization of translation invariant mmd on rd and connections with wasserstein distances. *Journal of Machine Learning Research*, 25(237):1–39, 2024. 3

[57] Yingwei Pan, Ting Yao, Yehao Li, Yu Wang, Chong-Wah Ngo, and Tao Mei. Transferrable prototypical networks for unsupervised domain adaptation. In *Proceedings of the IEEE/CVF conference on computer vision and pattern recognition*, pages 2239–2247, 2019. 11

[58] Zhongyi Pei, Zhangjie Cao, Mingsheng Long, and Jianmin Wang. Multi-adversarial domain adaptation. In *Thirty-Second AAAI Conference on Artificial Intelligence*, 2018. 4, 11

[59] Duo Peng, Qiuhong Ke, ArulMurugan Ambikapathi, Yasin Yazici, Yinjie Lei, and Jun Liu. Unsupervised domain adaptation via domain-adaptive diffusion. *IEEE Transactions on Image Processing*, 2024. 4

[60] Xingchao Peng, Qinxun Bai, Xide Xia, Zijun Huang, Kate Saenko, and Bo Wang. Moment matching for multi-source domain adaptation. In *Proceedings of the IEEE/CVF international conference on computer vision*, pages 1406–1415, 2019. 2, 8

[61] Kuniaki Saito, Kohei Watanabe, Yoshitaka Ushiku, and Tatsuya Harada. Maximum classifier discrepancy for unsupervised domain adaptation. In *Proceedings of the IEEE conference on computer vision and pattern recognition*, pages 3723–3732, 2018. 11

[62] Swami Sankaranarayanan, Yogesh Balaji, Carlos D Castillo, and Rama Chellappa. Generate to adapt: Aligning domains using generative adversarial networks. In *Proceedings of the IEEE conference on computer vision and pattern recognition*, pages 8503–8512, 2018. 11

[63] Yang Song, Jascha Sohl-Dickstein, Diederik P Kingma, Abhishek Kumar, Stefano Ermon, and Ben Poole. Score-based generative modeling through stochastic differential equations. *arXiv preprint arXiv:2011.13456*, 2020. 4

[64] Baochen Sun and Kate Saenko. Deep coral: Correlation alignment for deep domain adaptation. In *European Conference on Computer Vision*, pages 443–450. Springer, 2016. 3, 11

[65] Yulin Sun, Weisheng Dong, Xin Li, Le Dong, Guangming Shi, and Xuemei Xie. Transvqa: Transferable vector quantization alignment for unsupervised domain adaptation. *IEEE Transactions on Image Processing*, 33:856–866, 2024. 2, 4, 5

[66] Song Tang, An Chang, Fabian Zhang, Xiatian Zhu, Mao Ye, and Changshui Zhang. Source-free domain adaptation via target prediction distribution searching. *International journal of computer vision*, 132(3):654–672, 2024. 3

[67] Francesco Tonolini, Jack Radford, Alex Turpin, Daniele Faccio, and Roderick Murray-Smith. Variational inference for computational imaging inverse problems. *Journal of Machine Learning Research*, 21(179):1–46, 2020. 2

[68] Eric Tzeng, Judy Hoffman, Kate Saenko, and Trevor Darrell. Adversarial discriminative domain adaptation. In *Computer Vision and Pattern Recognition (CVPR)*, volume 1, page 4, 2017. 3, 11

[69] Hadi Vafaii, Dekel Galor, and Jacob Yates. Poisson variational autoencoder. *Advances in Neural Information Processing Systems*, 37:44871–44906, 2024. 7

[70] Aaron Van Den Oord, Oriol Vinyals, et al. Neural discrete representation learning. *Advances in neural information processing systems*, 30, 2017. 8

[71] Vladimir Vapnik. *The nature of statistical learning theory*. Springer science & business media, 1999. 5

[72] Hemanth Venkateswara, Jose Eusebio, Shayok Chakraborty, and Sethuraman Panchanathan. Deep hashing network for unsupervised domain adaptation. *arXiv preprint arXiv:1706.07522*, 2017. 8, 10, 12

[73] Hui Wang, Liangli Zheng, Hanbin Zhao, Shijian Li, and Xi Li. Unsupervised domain adaptation with class-aware memory alignment. *IEEE Transactions on Neural Networks and Learning Systems*, 2024. 2, 4, 5

[74] Jindong Wang, Wenjie Feng, Yiqiang Chen, Han Yu, Meiyu Huang, and Philip S Yu. Visual domain adaptation with manifold embedded distribution alignment. In *2018 ACM Multimedia Conference on Multimedia Conference*, pages 402–410. ACM, 2018. 2

[75] Shanshan Wang, Lei Zhang, Pichao Wang, MengZhu Wang, and Xingyi Zhang. Bp-triplet net for unsupervised domain adaptation: A bayesian perspective. *Pattern Recognition*, 133:108993, 2023. 11

[76] Ximei Wang, Liang Li, Weirui Ye, Mingsheng Long, and Jianmin Wang. Transferable attention for domain adaptation. In *Proceedings of the AAAI Conference on Artificial Intelligence*, volume 33, pages 5345–5352, 2019. 11

[77] Yixin Wang, David Blei, and John P Cunningham. Posterior collapse and latent variable non-identifiability. *Advances in neural information processing systems*, 34:5443–5455, 2021. 2, 5, 7

[78] Shaoan Xie, Zibin Zheng, Liang Chen, and Chuan Chen. Learning semantic representations for unsupervised domain adaptation. In *International conference on machine learning*, pages 5423–5432. PMLR, 2018. 11

[79] Tongkun Xu, Weihua Chen, Pichao Wang, Fan Wang, Hao Li, and Rong Jin. Cdtrans: Cross-domain transformer for unsupervised domain adaptation. *arXiv preprint arXiv:2109.06165*, 2021. 11
[80] Zihao Xu, Guang-Yuan Hao, Hao He, and Hao Wang. Domain-indexing variational bayes: Interpretable domain index for domain adaptation. In *The Eleventh International Conference on Learning Representations*, 2023. 4
[81] Jinyu Yang, Jingjing Liu, Ning Xu, and Junzhou Huang. Tvt: Transferable vision transformer for unsupervised domain adaptation. In *Proceedings of the IEEE/CVF winter conference on applications of computer vision*, pages 520–530, 2023. 11
[82] Xiangli Yang, Zixing Song, Irwin King, and Zenglin Xu. A survey on deep semi-supervised learning. *IEEE Transactions on Knowledge and Data Engineering*, 2022. 4
[83] Yanchao Yang and Stefano Soatto. Fda: Fourier domain adaptation for semantic segmentation. In *Proceedings of the IEEE/CVF Conference on Computer Vision and Pattern Recognition*, pages 4085–4095, 2020. 3
[84] Cheng Zhang, Judith Bütepage, Hedvig Kjellström, and Stephan Mandt. Advances in variational inference. *IEEE transactions on pattern analysis and machine intelligence*, 41(8):2008–2026, 2018. 2
[85] Jingyi Zhang, Jiaxing Huang, Zichen Tian, and Shijian Lu. Spectral unsupervised domain adaptation for visual recognition. In *Proceedings of the IEEE/CVF Conference on Computer Vision and Pattern Recognition*, pages 9829–9840, 2022. 11
[86] Kun Zhang, Mingming Gong, Petar Stojanov, Biwei Huang, Qingsong Liu, and Clark Glymour. Domain adaptation as a problem of inference on graphical models. *Advances in neural information processing systems*, 33:4965–4976, 2020. 4
[87] Qiming Zhang, Jing Zhang, Wei Liu, and Dacheng Tao. Category anchor-guided unsupervised domain adaptation for semantic segmentation. *Advances in neural information processing systems*, 32, 2019. 2, 4
[88] Yechuan Zhang, Jian-Qing Zheng, and Michael Chappell. Bayesian inference for non-linear forward model by using a vae-based neural network structure. *IEEE Transactions on Signal Processing*, 2024. 7
[89] Sicheng Zhao, Bo Li, Xiangyu Yue, Yang Gu, Pengfei Xu, Runbo Hu, Hua Chai, and Kurt Keutzer. Multi-source domain adaptation for semantic segmentation. In *Advances in Neural Information Processing Systems*, pages 7285–7298, 2019. 4
[90] Yewei Zhao, Hu Han, Shiguang Shan, and Xilin Chen. Deep subdomain alignment for cross-domain image classification. In *Proceedings of the IEEE/CVF Winter Conference on Applications of Computer Vision*, pages 2820–2829, 2024. 11
[91] Linqi Zhou, Aaron Lou, Samar Khanna, and Stefano Ermon. Denoising diffusion bridge models. *arXiv preprint arXiv:2309.16948*, 2023. 4
[92] Yongchun Zhu, Fuzhen Zhuang, Jindong Wang, Guolin Ke, Jingwu Chen, Jiang Bian, Hui Xiong, and Qing He. Deep subdomain adaptation network for image classification. *IEEE transactions on neural networks and learning systems*, 32(4):1713–1722, 2020. 2, 4, 11

Lingkun Luo served as a research assistant and postdoc at Ecole Centrale de Lyon, Department of Mathematics and Computer Science, and was a member of the LIRIS laboratory. He is currently a research fellow at Shanghai Jiao Tong University. He has authored over 40 research articles, including publications in *IEEE Transactions on Pattern Analysis and Machine Intelligence*, *International Journal of Computer Vision*, *ACM Computing Surveys*, *IEEE Transactions on Image Processing*, *IEEE Transactions on Cybernetics*, *IEEE Transactions on Information Forensics and Security*, *International Joint Conference on Artificial Intelligence* and others. His research interests include machine learning, pattern recognition, and computer vision.

Shiqiang Hu is a Full Professor and Dean of the School of Aeronautics and Astronautics at Shanghai Jiao Tong University. He has led numerous research projects funded by the National Science Foundation and the 863 National High Technology Program. He has published over 300 papers and supervised more than 30 Ph.D. students. His research interests include machine learning, image understanding, and nonlinear filtering.

Liming Chen is a Distinguished Professor in the Department of Mathematics and Computer Science at École Centrale de Lyon, University of Lyon, France, and a Senior Member of the Institut Universitaire de France (IUF). He received his B.Sc. from the University of Nantes in 1984 and his M.Sc. and Ph.D. in Computer Science from University Pierre and Marie Curie (Paris 6) in 1986 and 1989, respectively. He previously served as an Associate Professor at Université de Technologie de Compiègne and held positions at Avivias and France Telecom R&D China. His research interests include computer vision, machine learning, and multimedia, with a focus on robot vision and learning. He has published over 300 papers, supervised more than 40 Ph.D. students, and received funding from EU FP programs and national agencies. He is an Associate Editor for the *EURASIP Journal on Image and Video Processing*, an Area Editor for *Computer Vision and Image Understanding*, and a Senior Member of IEEE.